Influence of Acoustic Cavitation on the Controlled Ultrasonic Dispersion of Carbon Nanotubes

Achilleas Sesis[†], *Mark Hodnett*[†], *Gianluca Memoli*[†], *Andrew J. Wain*[†], *Izabela Jurewicz*[‡], *Alan B. Dalton*[‡], *J. David Carey*[§] *and Gareth Hinds*[†*]

[†]National Physical Laboratory, Teddington, Middlesex, TW11 0LW, United Kingdom

[‡]Department of Physics, University of Surrey, Guildford, Surrey, GU2 7XH, United Kingdom

[§]Advanced Technology Institute, University of Surrey, Guildford, Surrey, GU2 7XH, United Kingdom

ABSTRACT

Ultrasonication is the most widely used technique for the dispersion of a range of nanomaterials, but the intrinsic mechanism which leads to stable solutions is poorly understood with procedures quoted in the literature typically specifying only extrinsic parameters such as nominal electrical input power and exposure time. Here we present new insights into the dispersion mechanism of a representative nanomaterial, single-walled carbon nanotubes (SW-CNTs), using a novel up-scalable sonoreactor and an *in situ* technique for the measurement of acoustic cavitation activity during ultrasonication. We distinguish between stable cavitation, which leads to chemical modification of the surface of the CNTs, and inertial cavitation, which favors CNT exfoliation and length reduction. Efficient dispersion of CNTs in aqueous solution is found to be dominated

by mechanical forces generated via inertial cavitation, which in turn depends critically on surfactant concentration. This study highlights that careful measurement and control of cavitation rather than blind application of input power is essential in the large volume production of nanomaterial dispersions with tailored properties.

KEYWORDS: carbon nanomaterials, sonochemistry, surfactant, ultrasound

A. INTRODUCTION

A key area of nanotechnology development is the processing of functional nanomaterials[1,2]. Single-walled carbon nanotubes (SW-CNTs) have come to represent the prototype high aspect ratio nanomaterial and have been extensively studied due to their remarkable mechanical and electrical properties[3] for a wide range of potential applications[4] in biotechnology, composites and electronics. To take advantage of their intrinsic nanoscale properties in macroscale structures or devices, individually dispersed CNTs or small bundles are usually required. A significant material processing hurdle for CNTs, and other nanomaterials such as graphene, is the requirement to eliminate their strong tendency to agglomerate due to van der Waals interactions[5]. The primary chemical approach to stabilizing CNT dispersions is through the use of an appropriate solvent[6], with aqueous dispersions typically requiring an effective surfactant. A wide range of types of surfactant and concentrations have been investigated in the literature with various dispersion outcomes depending on the specific processes[7].

Ultrasonication has emerged as the prevailing technique for the dispersion of a range of nanomaterials. During ultrasonic processing in liquids the propagation of high amplitude ultrasonic pressure waves, typically generated using frequencies between 20 kHz and 1 MHz, leads to molecular dissociation, void creation and the rapid formation of cavities (bubbles). Continued interaction between bubbles and the acoustic field can result in their growth and ultimately, violent collapse. The implosion of bubbles can create local temperatures of several thousand kelvin and pressures of several hundred atmospheres[8]. During the growth and collapse phases sonochemical effects will occur, while extreme shear forces as well as optical and acoustic emissions are also generated[9-10]. Cavitation is a complex multi-parametric phenomenon that depends on the physicochemical properties of the liquid as well as the operational parameters of the ultrasonic device[11]. Studies of single-bubble interactions with CNTs have been limited to computational modeling[12], while more realistic multi-bubble systems have not been addressed. Until now, the effectiveness of ultrasonic dispersion has only been characterized by post-processing analysis of the CNTs[13] as a definitive metric for cavitation was not available.

Despite its critical role in the dispersion process, the fundamental mechanism of ultrasonic dispersion in complex environments is poorly understood and the role of acoustic cavitation often neglected by the materials science community. As a consequence, many of the dispersion strategies in the literature are empirical in nature and typically specify only the solute concentrations, the nominal electrical input power of the device and the exposure time. Moreover, this type of treatment may lead to unintentional and undesirable chemical and physical modification of the CNTs[14]. The need for a more systematic approach to the dispersion of nanomaterials and nanoparticles has been highlighted in a recent review article[15].

On the other hand, the effects of acoustic cavitation can be monitored directly in near real-time using techniques such as sonoluminescence and acoustic emission or indirectly by evaluating the yield of chemical by-products and monitoring erosion of surfaces[11]. With bubbles in solution behaving as secondary sound sources, it is possible to interpret the acoustic emission spectra in terms of bubble growth and implosion behavior[10] and therefore link a macroscopic signal to what is happening at the nanoscale. In this context, the National Physical Laboratory (NPL) has pioneered the development of a reference cavitation facility[16] to understand the underlying physics of cavitation.

In this work we apply a modified NPL cavitation sensor[17] to the *in situ* investigation of the fundamental CNT dispersion mechanisms. We demonstrate unequivocally the importance of cavitation activity measurement and the identification of the cavitation type, for understanding and controlling the dispersion of CNTs. The effects of ultrasonication on the surfactant as well as a means to controllably adjust the nanotube length are also examined. Our conclusions are not limited to carbon nanotubes and can be applied to any nanomaterial systems in which van der Waal interactions are important.

B. EXPERIMENTAL

Solution Preparation. Air-saturated stock solutions of 0.72 mM (30% cmc) and 7.2 mM (300% cmc) of sodium deoxycholate (NaDOC) (Thermo Scientific) in Milli-Q™ water (18.2 MΩ cm, < 5 ppb T.O.C.) were prepared prior to each experiment by magnetic stirring at 1000 rpm for 1 hour at 25 °C. Prior to the cavitation measurements 10 mL aliquots of the stock solution were ultrasonicated in a 15 mL polypropylene non-skirted centrifugation tube (Fisher Scientific) in the 25 kHz reference vessel[16]. In this case the tube was partly immersed up to the 15 mL mark along

the central axis of the 25 L vessel and a 15 minute, 100 W exposure was used. Hereafter this process is termed Pretreatment. A schematic of this configuration is shown in the Supporting Information (Figure S1a). When CNTs (SRM-2483, N.I.S.T., USA) were used, in order to accelerate the dispersion process within the reactor, a total mass of 5 mg was added to the 10 mL solution to undergo the pretreatment process. The pretreated solutions were then mixed with 240 mL of the respective stock solution to form a reactor liquid volume of 250 mL. When CNTs were used the starting concentration was 0.02 $mg.mL^{-1}$. At fixed intervals (0, 15, 30 and 60 minutes) 1 mL aliquots were extracted for chemical analysis (H_2O_2), CNT quality and dispersion characterization. In order to minimize the exposure time of the sensor to the acoustic field, during cavitation measurements the reactor lid was replaced with an identical lid, to which the cavitation sensor was attached.

In Situ **Measurement of Ultrasonic Cavitation and Temperature.** A modified NPL cavitation sensor was housed within the custom-built reactor at a fixed height of 35 mm from the inner side of the lid. The reactor was positioned in the vessel at a fixed height (the center of the reactor body was 40 mm below the water surface) along the central axis of the reference vessel. One row of ten equally spaced transducers around the top of the reference vessel was used to apply the acoustic field throughout this work. The nominal input power was equally distributed between the ten transducers. During acoustic cavitation experiments the sensor was connected to a spectrum analyzer (HP3589A, Hewlett Packard) and emission signals were recorded for an average of 128 sweeps over the frequency range 2 MHz to 4 MHz. Integration was performed on each acquired spectrum to determine the broadband integrated energy using Equation 1. The temperature of both the reactor solution and the vessel solution was also recorded at 10 second intervals using PEEK-sheathed mini T-type stainless steel 0.5 mm thermocouples (Omega

Engineering) connected to a temperature data logger (MMS3000 T6VA, ISE). These thermographs were then analyzed using calorimetry to estimate the effective power dissipated within the reactor. The vessel water temperature remained in the range 33.0 ± 0.5 °C throughout the tests. Using an identical configuration the reactor was also set up to acquire data on the cavitation activity associated with a sonotrode (20 kHz, P100, Sonic Systems) with a tip diameter of 15 mm (Figure S1b). In these tests the reactor solution temperature was 26.7 ± 0.9 °C and the volume of air-saturated Milli-Q™ water was 300 mL. The vertical distance between the probe tip and sensor surface was fixed at 50 mm, while the tip was centered with respect to the vial and sensor. All acoustic data were acquired over a 2 minute period and averaged over four to eight independent measurements.

H_2O_2 Chemical Assay. Absorption spectroscopy (Cary 5000 UV-Vis-NIR, Agilent Technology) was used to measure H_2O_2 concentration in the treated solutions using a peroxide assay kit (PeroXOquant™, Thermo Scientific). 50 μL of the sample was mixed with the 500 μL assay immediately after its extraction from the reactor and left to stand for 24 hours at 20 °C, in airtight 10 mm disposable cuvettes (UV-Cuvette micro 8.5 mm, BRAND). The absorbance of the solution was then measured at 585 nm and compared against a calibration curve produced from samples with a known concentration of H_2O_2.

Resonance micro-Raman Spectroscopy. For all ultrasonicated samples, 1 mL aliquots were left to stand for 24 hours at 20 °C to allow large CNT bundles to sediment under stagnant conditions. 50 μL aliquots from the supernatant were then deposited on silicon wafer substrates and left to dry in air. For the untreated samples, measurements were conducted directly on the as-received CNT powder. For all samples an average of 10 scans at various points on the substrate was taken. The spectra were obtained using an excitation wavelength of 632.8 nm (1.96 eV), using a

RM 2000 microRaman spectrometer (Renishaw). The spectral resolution was 1 cm^{-1} and a 50× magnification objective lens was used; the spot size diameter was estimated to be approximately 1 μm with a nominal power of 1.25 mW (25% power intensity on the sample). Calibration was performed using a silicon wafer (520.5 cm^{-1} ± 0.5 cm^{-1}). Spectra were then background corrected by removing the silicon and surfactant intensity contributions within the G- and D-band regions of interest. The quality ratios were then evaluated on the normalized spectra.

Absorption Spectroscopy. Absorption spectroscopy (Cary 5000 UV-Vis-NIR, Agilent Technology) was used to evaluate the dispersion efficiency and relative fraction of individual CNTs for each ultrasonication. After each exposure 1 mL of sample was removed from the reactor and left to stand for 24 hours under stagnant sedimentation conditions at 20 °C. 400 μL of the supernatant was placed in airtight 10 mm disposable cuvettes (UV-Cuvette micro 15 mm, BRAND). The absorbance of the solution was then measured between 400 nm and 800 nm and the area ratio of the E_{22} resonance peak at ~570 nm to its non-resonant background was calculated.

Atomic Force Microscopy. 250 mL of CNT samples were left to stand for 24 hours at 20 °C to allow large CNT bundles to sediment under stagnant conditions. 40 μL supernatant aliquots of these solutions were spin-coated at 3000 rpm for 10 seconds onto freshly cleaved mica substrates and left to dry in air for 15 minutes. For topographic studies, an NTEGRA Prima AFM (NT-MDT) was used in semi-contact mode configuration. AFM probes (Nanosensors™) with force constants ranging from 10 N m^{-1} to 130 N m^{-1} were used. Several AFM topography and phase images were recorded for each sample and analyzed for length and diameter distribution histograms. All images were corrected for sample tilt using NOVA (NT-MDT) and a background subtraction was employed using a first-degree polynomial plane fitting for each line scan.

Surfactant Characterization. Air-saturated, stock solutions of 0.12 mM (50% cmc) Triton™ X-100 (TX) (BioXtra, Sigma-Aldrich) and 0.048 mM (2% cmc) sodium deoxycholate (NaDOC) (Thermo Scientific) in Milli-Q™ water (18.2 MΩ cm, < 5 ppb T.O.C.) were prepared prior to each experiment by magnetic stirring at 1000 rpm for 1 hour at 25 °C. Aliquots of 250 mL of each solution were ultrasonicated using the NPL reference vessel in the reactor using an applied nominal power of either 100 W or 200 W. The vessel water temperature remained in the range 33.0 °C ± 0.5 °C throughout the tests and the temperature within the reactor was monitored continuously. During the ultrasonication process 1 mL aliquots were extracted from the reactor at fixed time intervals. For the TX chemical analysis a reverse phase high performance liquid chromatograph (RP-HPLC) (JASCO) with a photodiode array (PDA) UV detector set at 224 nm was used. The system was configured to isocratic mode. The column used was a hydrophobic Kinetex™ 2.6 μm, C18, 100 Å, 4.6 mm (Phenomenex) and the mobile phase was 55:45 (% v/v) RP-HPLC grade CH_3CN/Milli-Q™. An injection sample volume of 90 μL at a flow rate of 1.5 mL min^{-1} was used; each sample had a runtime of approximately 5 minutes at room temperature. The integral of the TX HPLC trace was then converted to concentration in order to evaluate the loss of surfactant. For the chemical analysis of NaDOC, electrospray ionization mass spectrometry (ESI-MS) was conducted on a Thermo Scientific LTQ-Orbitrap Velos™ mass spectrometer with the highest resolution setting of 100,000 (at m/z 400), in the positive ion mode. A solution of 40:60:0.1 (% v/v) (sample:MS grade CH_3CN:HCO_2H) was prepared and injected at 0.5 μL min^{-1} using an electrospray voltage of 3.8 kV. The mass spectra were acquired for 3 minutes and the mass spectrometer was programmed to collect up to a maximum Orbitrap injection time of 500 ms, using an automatic gain control (AGC) setting of 5×10^5. The AGC is designed to fill the trap with the optimal amount of ions to ensure that the signal intensities are

high and that the spectra are not distorted by space-charging effects. Estimates of the molecular fragment structures were performed using XCalibur™ (Thermo Scientific) software set to a mass accuracy of 5 ppm.

Rheology Measurements. Measurements were taken using a (AR-G2, TA Instruments) rheometer at 23 °C, with a rotational plate applying a cyclic shear rate of 50 s^{-1} to 200 s^{-1}.

C. RESULTS AND DISCUSSION

Cavitation Measurements. In this work a unique acoustic measurement facility was established to achieve controlled ultrasonic conditions within the experimental solution volume. The ultrasonic source used was a 25 kHz-driven reference vessel[16] (Figure 1a), which was designed to produce repeatable acoustic cavitation of a known spatial distribution. The experimental solution was placed within the custom-built reactor (Figure 1b) located on the cylindrical vessel's central axis. The NPL cavitation sensor (Figure 1c) was housed in the reactor to measure the acoustic emissions from bubbles generated within the experimental volume. Key features of the frequency spectra, measured as a function of nominal electrical input power, are depicted in Figures 1d and 1e. At low input power a low driving acoustic pressure amplitude causes the bubble wall to oscillate linearly and only the fundamental driving frequency (f_o = 25 kHz) is observed. The degree of nonlinear oscillation increases as a function of driving pressure (typically via the increase of input electrical power), leading to the generation of various additional peaks[10,17], amongst which is the first sub-harmonic, observed here at $f_o/2$ = 12.5 kHz (Figure 1d). Further increases to the driving pressure lead to chaotic bubble oscillation and ultimately bubble collapse, which is demonstrated by the rising broadband noise level well into the MHz region (Figure 1e). It is generally accepted[10] that this broadband noise is associated with

inertial (also known as transient) cavitation (Figure 1f), whereby bubbles collapse chaotically within a few pressure wave cycles. This is in contrast to stable cavitation (Figure 1f), whereby bubbles undergo multiple oscillations and do not necessarily collapse, but can grow and be forced out of the liquid volume due to buoyancy[18].

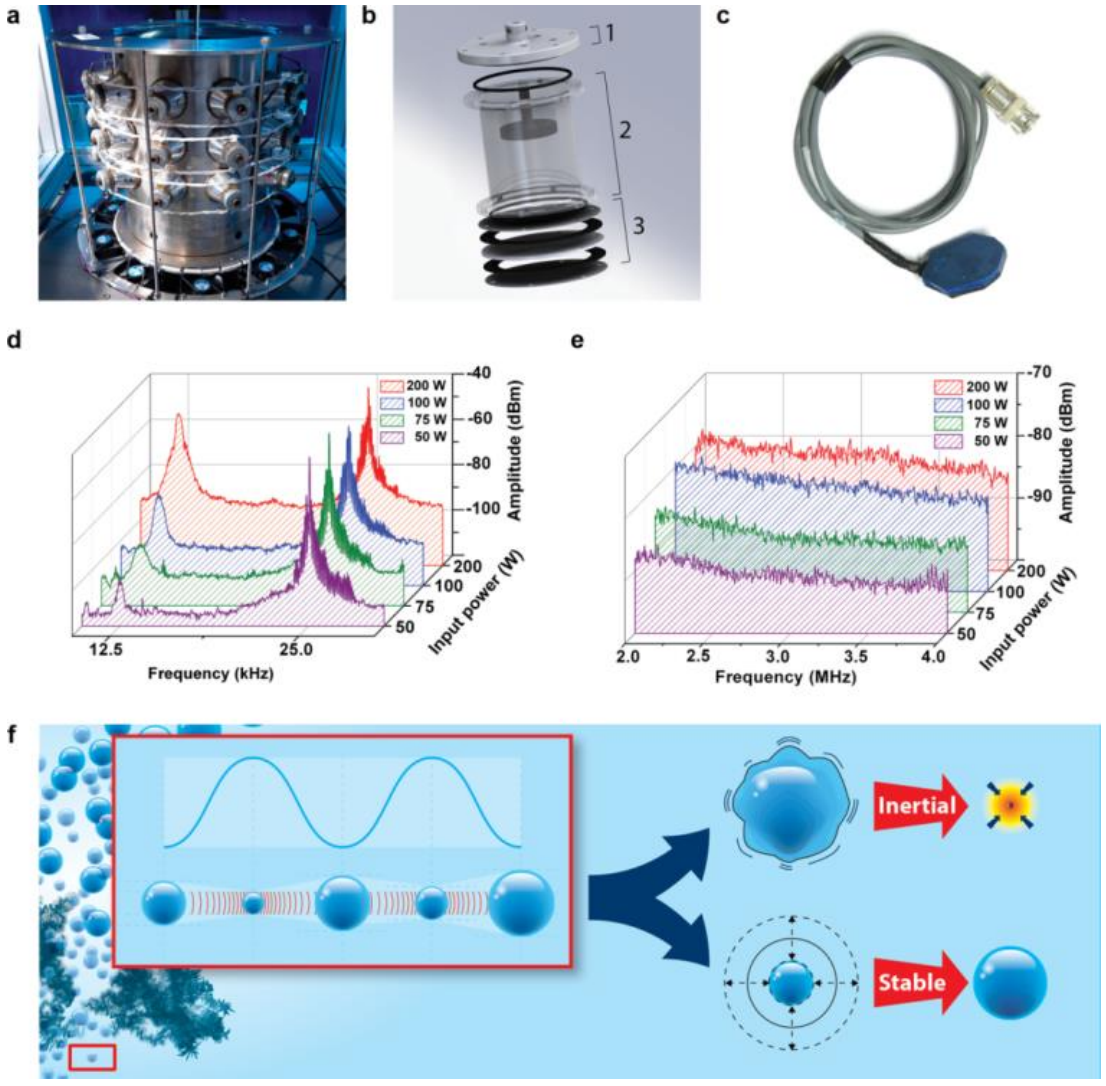

Figure 1. Novel experimental apparatus. **a,** NPL's 25 L, 25 kHz - frequency driven reference ultrasonic vessel. **b,** Computer-aided design of the custom-built reactor, where the lid (1) and main body (2) are made from polycarbonate and the base (3) is a ceramic-nylon sandwich layer. The maximum reactor volume is 370 mL. **c,** NPL's cavitation sensor with a thickness of 5.5 mm and a surface area of ~10 cm^2 housed within the reactor during experiments. **d,** Low frequency acoustic emission spectra taken with the cavitation sensor, showing the effect of input power on the f_0 and $f_0/2$ peaks as well as the broadband noise. **e,** High frequency region of the spectrum showing a clear increase of broadband noise with input power. **f,** Left: illustration of the multi-bubble cloud typically generated in ultrasonically treated solutions. Right: Schematic of the two types of cavitation mechanism.

The presence of the sub-harmonic peak, even at the lowest input power used in this work, indicates that the acoustic pressure amplitude in the selected measurement region is close to the inertial cavitation threshold. However there remains some debate over whether the amplitude of the sub-harmonic peak can be used as a measure of inertial cavitation[10] and therefore a more definitive metric is required. Studies of the high frequency (MHz) region have shown that the energy associated with the broadband acoustic emission spectrum is a practical metric for inertial cavitation activity[17]. This is parameterized by the term E_{cav}, which is evaluated by integrating the square of the magnitude of the sensor response, $V_c(f)^2$, between two frequencies f_1 and f_2, chosen to ensure that a significant fraction of the acoustic energy residing in the MHz region is acquired.

$$E_{cav} = \int_{f_1}^{f_2} V_c(f)^2 df \quad (1)$$

Measurements of E_{cav} in the frequency range of 2 MHz to 4 MHz are shown in Figure 2 with additional data shown in Figure S2. The reactor experiments were performed using aqueous anionic surfactant sodium deoxycholate (NaDOC) solution, which is known to facilitate improved dispersion of SW-CNTs[7,19]. Tests were conducted with and without CNTs[20]. The effect of surfactant concentration on the acoustic field above (300%) and below (30%) the critical micelle concentration (cmc) of NaDOC was investigated by measurement of the cavitation activity.

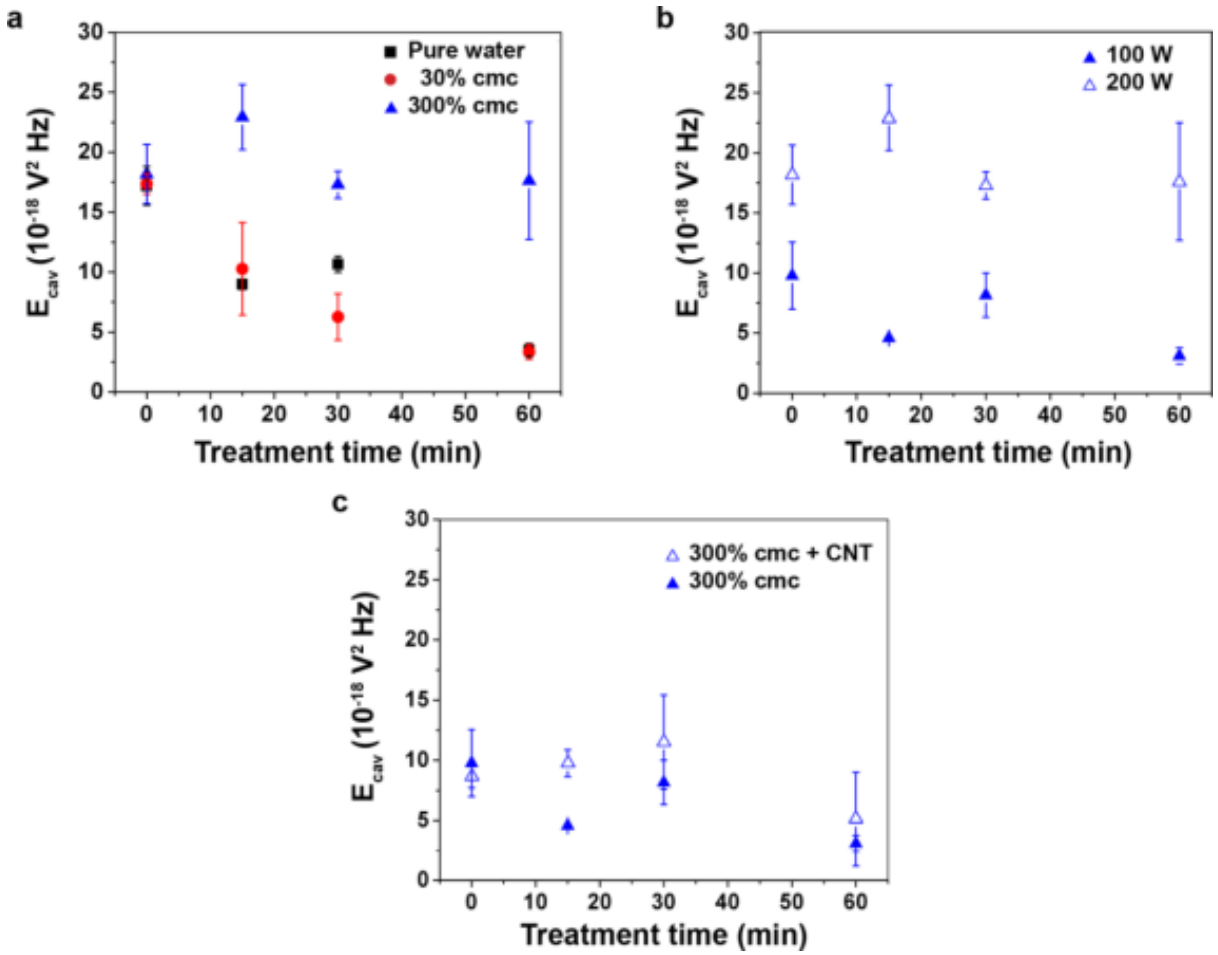

Figure 2. *In situ* cavitation measurements. **a,** Cavitation activity as a function of time for different surfactant (NaDOC) concentrations in the absence of CNTs during 60 minute tests at 200 W. **b,** Cavitation activity as a function of time for different input powers for the 300% cmc solutions in the absence of CNTs. **c,** Cavitation activity as a function of time at 100 W for a 300% cmc solution in the absence and presence of 0.02 mg mL^{-1} CNTs.

No significant difference is observed between E_{cav} measurements in pure water and those in 30% cmc surfactant (Figure 2a), which suggests that the population of inertial cavitation bubbles at 30% cmc is similar to that found in pure water and that any excess bubbles are experiencing stable cavitation. The error bars indicate the short-time measurement variability associated with the stochastic nature of inertial cavitation. By contrast, after 60 minutes of ultrasonication the level of inertial cavitation at 300% cmc is significantly higher than that at 30% cmc, for example

by approximately a factor of four at 200 W. This observation highlights the remarkable sensitivity of cavitation activity to solution composition. Since a negligible background activity was observed at 0 W, a non-linear relationship exists between inertial cavitation activity and nominal input power (Figure 2b), highlighting an intrinsic limitation in the widespread use of input power as a primary experimental parameter. A similar non-linear behavior is evident in the broadband response shown in Figure 1d. No significant effect of the presence of CNTs was observed in the cavitation measurements (Figure 2c) under these conditions, which implies that the CNT concentration used in this study was sufficiently low that the measured acoustic field was moderately unperturbed.

A notable feature of the data in Figure 2a is that the magnitude of E_{cav} remains relatively constant for the 300% cmc solution but decreases with exposure time in both pure water and in 30% cmc solution. Inertial cavitation is clearly favored at the higher surfactant concentration, which may be ascribed to more facile formation of bubbles due to the reduced surface tension. Furthermore it is believed that at 30% cmc the distance between bubbles is relatively large due to electrostatic repulsion[21]. When the ionic surfactant concentration is increased to 300% cmc, the concomitant increase in solution ionic strength leads to charge shielding effects, reducing the repulsion between surfactant molecules and resulting in the formation of denser bubble clouds. A similar hypothesis was previously proposed to rationalize acoustic measurements in an anionic surfactant[21]. A contributing factor to the decrease in inertial cavitation with time in pure water and at 30% cmc may be a preference for stable cavitation as the bulk solution temperature increases during ultrasonication[9,11].

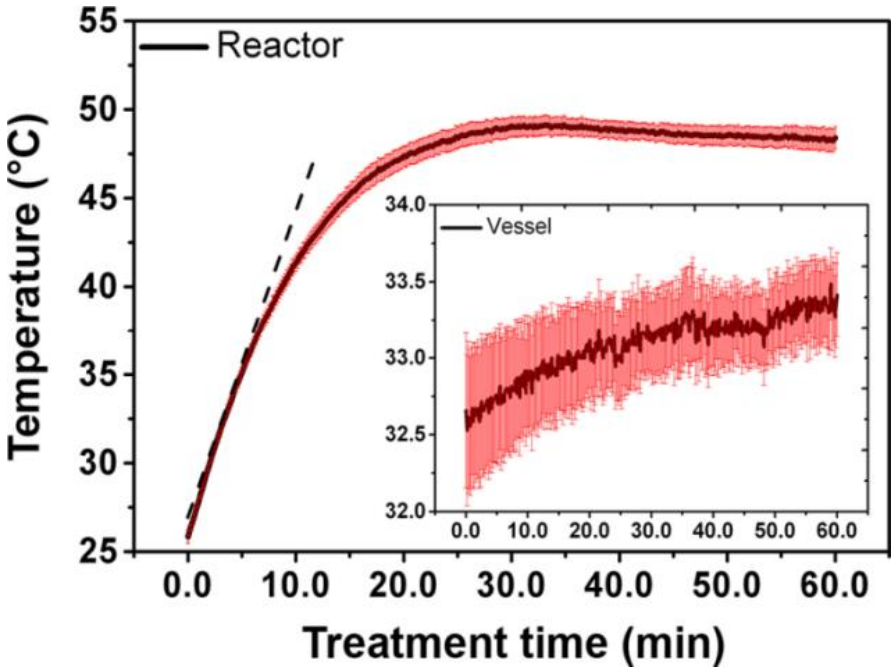

Figure 3. Average thermographs of the temperature within the reactor during the 200 W tests. Inset illustrates the vessel temperature profile. Error bars represent standard error between six independent measurements.

The average variation of solution temperature during ultrasonication at 200 W is shown in Figure 3. The temperature increases from its initial value of ~25 °C and reaches steady state value of ~48 °C after approximately 30 minutes; a similar trend is observed at 100 W (see Figure S3) with a lower steady state temperature of ~41 °C. This temperature increase will enhance bubble formation due to the increase of vapor pressure. However at 30% cmc the more widely spaced bubbles will grow via the mechanism of rectified diffusion[9], whereby growth is achieved as a result of uneven mass transfer across the bubble/solution interface. Degassing can then occur via bubble coalescence and removal from the liquid due to buoyancy, hence reducing the number of bubble nucleation sites. By contrast, the 300% cmc solution could enhance the number of cavitation nucleation sites due to the high concentration of micelles. In addition, the use of a low frequency device (25 kHz) will favor a more significant increase in the population of bubbles

undergoing inertial cavitation at the higher surfactant concentration[22]. This effect is enhanced by the denser bubble population at 300% cmc.

The fraction of the nominal input power that is converted to thermal energy may be determined by calorimetric analysis of the thermographs (see Supporting Information). At 100 W, 35% of the input power is converted to heat; this falls to 25% at 200 W. No linear dependence of amount of cavitation on the input thermal energy was observed, implying that input thermal power is an equally unsatisfactory indicator of the amount of cavitation in solution. This non-linearity is due to non-uniformities in the acoustic field partially arising from system geometry and the acoustic properties of the container material. Other indirect metrics for cavitation level such as energy density have been proposed in the literature[23] but this study demonstrates that caution should be applied to the use of any metric that is based on calorimetric determination of the acoustic energy. For example, if the cavitation distribution is non-uniform in the treated volume, a comparison of two systems based on calorimetric measurement may be misleading.

Comparison with Tip Ultrasonication. Routine approaches to CNT dispersion often utilize an ultrasonic tip, as opposed to a bath, so it is pertinent to compare the E_{cav} values from the reference vessel with those obtained from a commonly used bench top sonotrode. As shown in Figure 4, a maximum in E_{cav} is reached between 10 W and 15 W before a steady decline of cavitation activity is observed, approaching background levels at 50 W. The decrease in E_{cav} with increasing input power is due to cavitation shielding[11], where the increasing population of coalescing bubbles immediately beneath the tip leads to formation of air pockets surrounded by a stagnant region.

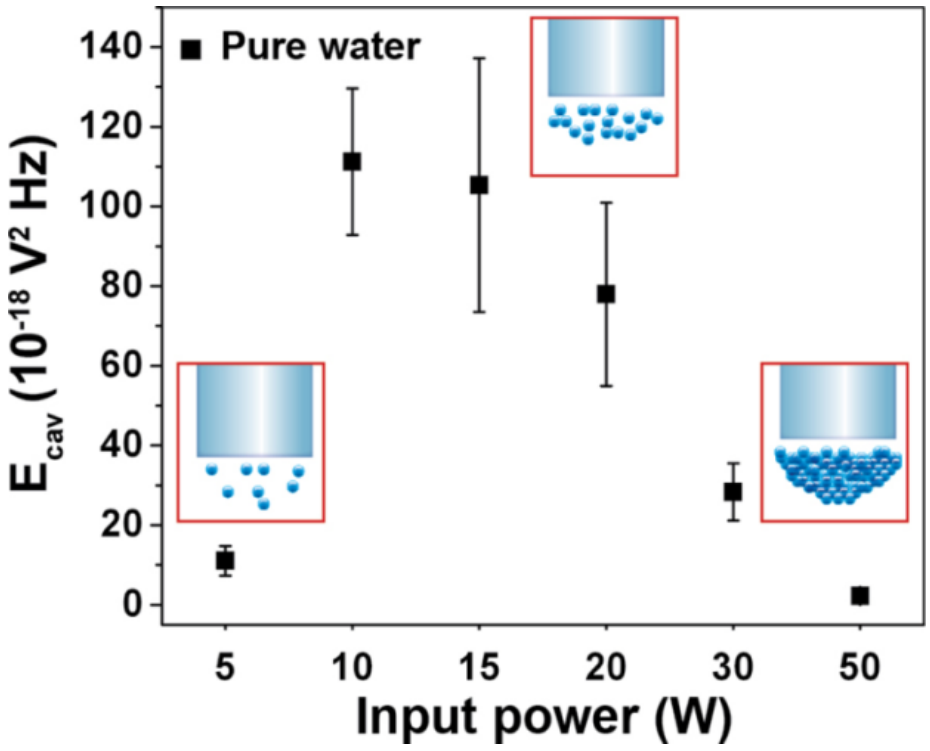

Figure 4. Cavitation activity measured for a tip ultrasonic device as a function of input power. Insets illustrate the variation of bubble population in the vicinity of the tip in three distinct regions of the graph. Error bars represent standard error between four to eight independent measurements.

This hinders the transmission of acoustic waves and the generation of inertial cavitation. The non-linear response with input power and its potential variation across ultrasonication devices present a barrier to the intelligent selection of treatment parameters. The E_{cav} levels determined in the sonotrode and reactor measurements may be compared directly, as they are made with the same sensor, in the same container and with a similar medium. The peak E_{cav} levels observed with the sonotrode are approximately an order of magnitude higher than in the reactor, which shows that even at modest input powers tip sonication is significantly disruptive. The sonotrode output is applied directly to the fluid through a 15 mm diameter tip, which vibrates with a displacement of up to 15 μm. This generates locally high acoustic pressures, which in turn cause intense inertial cavitation, but over a very small region, i.e. a few millimeters below the tip. For

equivalent powers, the reactor wall displaces less than 1 μm, but still generates acoustic pressures sufficient to cause inertial cavitation over a much larger fluid volume. With the acoustic field and the consequent cavitation activity generated by a larger number of acoustic sources, i.e. the vessel's ten equidistantly spaced transducers, a more even cavitation field is generated and the likelihood of cavitation shielding is reduced. Thus, the reactor generates a far more uniform cavitation distribution than the sonotrode and potentially a better 'nanoparticle dispersion stimulus' within a larger solution volume. The sonotrode has the additional disadvantage of contamination of the solution with metal fragments eroded from the tip[11]. These considerations point to significant advantages for industrial scale-up of such batch processing.

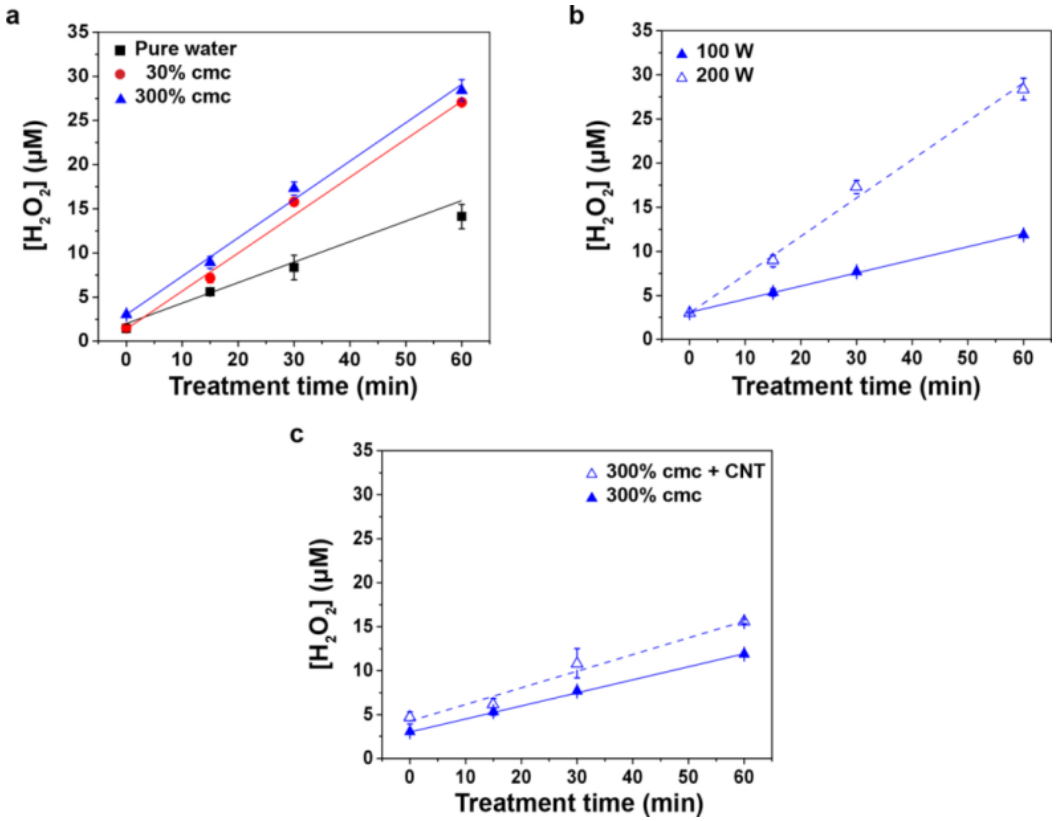

Figure 5. Sonochemical generation of hydrogen peroxide. **a,** H_2O_2 concentration as a function of time for different surfactant concentrations in the absence of CNTs during 60 minute tests at 200 W. **b,** H_2O_2 concentration as a function of time for different input powers for the 300% cmc solutions in the absence of CNTs. **c,** H_2O_2 concentration as a function of time at 100 W for a 300% cmc solution in the absence and presence of 0.02 mg mL^{-1} CNTs. Error bars represent standard error between four independent measurements.

Hydrogen Peroxide Measurements. Measurement of reactive oxygen species (ROS) such as hydrogen peroxide (H_2O_2) generated by ultrasonication can be used as a quantitative indicator of cavitation activity[9,11]. The cumulative concentration of H_2O_2 measured under the same conditions as the *in situ* acoustic measurements is presented in Figure 5 with additional data shown in the Supporting Information (Figure S4). In all cases a linear trend of H_2O_2 concentration with time is observed. The results are in marked contrast to the acoustic data in Figure 2. Firstly, the most significant change in the rate of production of H_2O_2 is observed between pure water and the 30% cmc solution, rather than between the two surfactant concentrations (Figure 5a). Secondly, the rate of generation of H_2O_2 varies approximately linearly with input power (Figure 5b). Thirdly, an effect (albeit modest) of CNT presence is observed (Figure 5c).

The apparent discrepancy between the acoustic data and the H_2O_2 concentration measurements may be explained on the basis of inertial vs. stable cavitation. The highly spaced bubbles in the 30% cmc solution will undergo stable cavitation activity assisted by the thermal effects discussed above and act as micro-reactors for H_2O_2 formation[24], which explains the marked increase of H_2O_2 generation compared to pure water. Importantly this does not exclude the formation of inertial bubbles, since higher than background activities were recorded (Figure 2a).

These observations suggest that the predominant route to H_2O_2 formation is in fact stable cavitation, as opposed to inertial cavitation, and that the excess surfactant might behave as a primary micelle radical trap[21] or radical scavenger[25], as evidenced by the comparably small apparent increase in H_2O_2 formation between 30% and 300% cmc surfactant. The relatively

small systematic increase in H_2O_2 concentration due to the presence of CNTs (Figure 5c) suggests that the CNTs (at the low concentration used in this work) have only a minor role in the formation of bubbles undergoing stable cavitation. Trapped air within the CNT agglomerates released during debundling, coupled with the increased number of nucleation sites due to the additional surface area, may in fact provide additional sources of stable cavitation.

Surfactant Degradation. Another key finding of our study is the degradation of surfactant as a result of ultrasonication. Chemical characterization of 2% cmc NaDOC solution using mass spectroscopy (MS) demonstrates the growth of new molecular fragments and their increase in concentration with ultrasonication time and input power (Figure 6a). These fragments can be assigned to specific products (see Table S1) resulting from the oxidative dehydrogenation and dehydration of the parent NaDOC molecule, initiated by ROS. Similar damage is observed to a non-ionic surfactant, Triton® X-100 (TX), which is also commonly used in the literature as a CNT dispersant. In this case the HPLC analysis indicated a gradual decrease in TX concentration when subjected to ultrasonication (Figure 6b). The reduction in spectral intensity with increasing exposure time and input power can be attributed to the degradation of the chromophore-bearing hydrophobic segment (Figure S5). A similar process is used in water treatment to destroy undesirable surfactants via pyrolytic bond cleavage and ROS chemical attack[26], although this typically employs much higher frequencies (hundreds of kHz). Our results show that ultrasonic degradation of surfactants is clearly also an issue of concern at lower frequencies and its exact impact on dispersion efficiency will require more detailed studies of surfactant-CNT surface interactions as demonstrated elsewhere[27]. However, at 30% cmc and 300% cmc of NaDOC no distinctive fragments were observed in the MS analysis, which may be a result of the increased turbidity of these solutions as discussed below.

Visual observation of the surfactant-water solutions (i.e. in the absence of CNTs) revealed a steadily increasing turbidity with ultrasonication time. To our knowledge this effect has not been previously reported in the literature on CNT dispersion, most likely because CNTs are always present in such studies, typically at relatively high concentrations. Turbidity of a surfactant solution may occur as a result of the dehydration of the hydrophilic segment of the surfactant as the bulk solution temperature increases, leading to the formation of close packed structures and phase separation within the liquid[28]. This behavior raises a number of questions regarding the effectiveness of NaDOC as a CNT dispersant, as well as its effect on bubble dynamics. Rheology measurements showed a correlation between the extent of ultrasonic treatment and viscosity (Figure 6c). The magnitude of the increase in viscosity was modest in absolute terms, with a maximum of ~3% for the higher surfactant concentration after 60 minutes at 200 W. Nevertheless, a trend with increasing exposure conditions can be discerned.

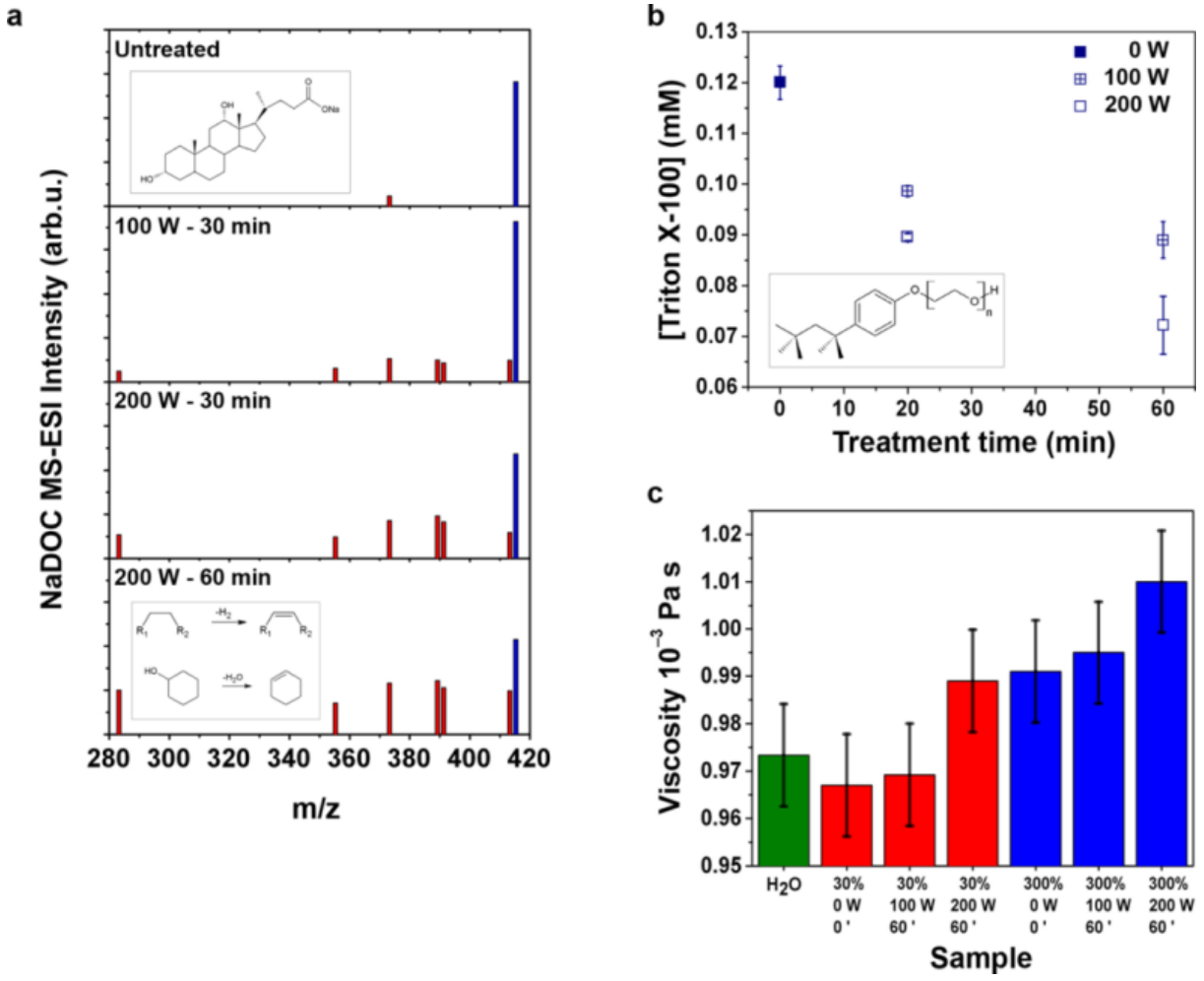

Figure 6. Sonochemical effects on two common CNT-dispersing surfactants. **a,** ESI-MS analysis of aqueous solutions of NaDOC (■), showing the generation of smaller molecular fragments (■) over time as a result of ultrasonication. Top inset illustrates the molecular structure of the pristine NaDOC molecule, bottom inset illustrates the proposed degradation reaction scheme for the oxidative dehydrogenation and dehydration of NaDOC. **b,** HPLC analysis of aqueous solutions of TX as a function of ultrasonication time for different applied powers. Inset illustrates the molecular structure of the pristine TX molecule. **c,** Dynamic viscosity measurements of NaDOC solutions compared to that of pure water. Error bars represent standard error between four independent measurements.

Carbon Nanotube Dispersion. The phase behavior of CNT dispersion is complex in nature[27]. In particular, aqueous based dispersions which use surfactant as a stabilizer require a subtle balance between surfactant and CNT concentrations. Often, dispersions that have been subjected to extended ultrasonication are unstable over time with the result that the CNTs eventually

sediment out of solution. This is illustrated in Figure 7a, which depicts 30% cmc (right vial) and 300% cmc (left vial) solution left standing for 14 days after ultrasonication for 60 minutes at 200 W. Whereas a uniform dispersion was maintained in the 300% cmc surfactant solution, significant sedimentation was observed at 30% cmc, indicating the critical role of the surfactant concentration. UV-Vis absorption spectroscopy may be used to characterize the quality of the CNT dispersion[29] and typically via the analysis of the resonance peak ratio[30]. This is depicted in Figure 7b for the two different surfactant concentrations treated at 200 W.

The drop observed from 0 to 15 minutes illustrates the re-agglomeration and sedimentation of the CNTs, which failed to disperse when the pretreated solution was stirred into the remaining reactor volume (see Experimental Section). Therefore, the dispersion is not at equilibrium and is dynamically changing; the resulting flocculation can occur via depletion driven aggregation[27], which depends on surfactant concentration as well as the interaction of the surfactant with the CNT lattice. Readings taken from 15 minutes onwards clearly show a gradual increase in the population of dispersed CNTs. A similar trend is observed at 100 W (Figure S6a). The ten-fold increase of surfactant concentration leads to the exfoliation of more CNTs, with an average increase in dispersion efficiency of ~25% at 100 W and ~80% at 200 W (Figure S6b and S6c respectively). CNT diameter and length histograms were determined from detailed analysis of representative AFM images after 60 minutes of exposure. Both exfoliation (Figure 7c) and length reduction (Figure 7d) are evident, with the reduction in CNT diameter and length more pronounced at 300% cmc and 200 W. The pretreated solutions are populated by a range of bundle sizes, up to 30 nm at 30% cmc and < 10 nm at 300% cmc. The effect of ultrasonication is to reduce the average bundle diameter significantly, to below 5 nm at 30% cmc and to below

3 nm at 300% cmc. Similar effects are observed on CNT length, for which the largest effect is observed at 300% cmc, with a ~36% average reduction in CNT length at 200 W within 60 minutes, compared to ~27% for all other exposures. The AFM data are summarized in an alternative format in Figure S7.

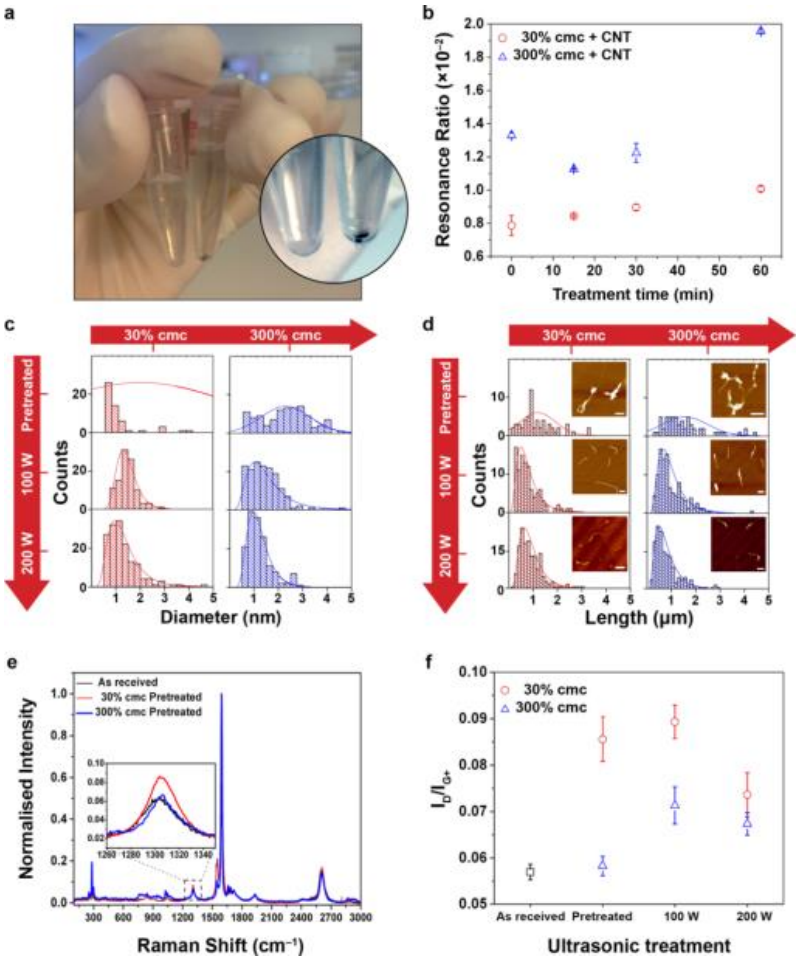

Figure 7. Characterization of CNT quality and dispersion. **a,** Photograph illustrating effect of surfactant concentration on CNT dispersion stability (left vial: 300% cmc, right vial: 30% cmc NaDOC). **b,** Optical absorption resonance ratio of the E_{22} resonance band for ultrasonically treated CNTs, indicating an increase in the concentration of singly-dispersed CNTs as a function of applied power and exposure time. **c,** CNT diameter measurements from AFM images of mica substrates spin-coated with solutions ultrasonically treated for 60 minutes as a function of surfactant concentration and input power. **d,** CNT length measurements from AFM images of mica substrates spin-coated with solutions ultrasonically treated for 60 minutes as a function of surfactant concentration and input power. Scale bars: 400 nm. **e,** Representative Raman spectra of dried CNTs before and after pre-treatment. **f,** Raman spectroscopy quality ratios (I_D/I_{G+}) for as-received and ultrasonically treated CNTs. Error bars represent standard error between four independent measurements.

Raman spectroscopy is used to determine the increase in defects[31] created by ultrasonication, indicated by the intensity ratio of the D-band to the G^+-band (I_D/I_{G^+}) as shown in the representative spectra in Figure 7e. Significant damage to the CNTs is observed during pretreatment at 30% cmc, but not at 300% cmc (Figure 7f). The general observation that the I_D/I_{G^+} ratio is affected by ultrasonication may be related to CNT damage via ROS attack[32]. The lower level of damage at 300% cmc is rationalized by the protective coating of the excess surfactant on the CNT surface, which will naturally form as the cmc point is surpassed. Interestingly, the I_D/I_{G^+} ratio is lower at 200 W than at 100 W for both surfactant concentrations, which is more marked for the 30% cmc sample. The AFM analysis indicates that the change in average length distribution between the two powers is not sufficient to explain the reduction in this ratio. It may however be a result of disruption of the long range order of the sp^2 carbon hexagonal as the number of point-like defect sites increases[33].

Implications. The acoustic and sonochemical measurements discussed above have significant implications for researchers wishing to control dispersion of nanomaterials for a wide range of applications. Ultrasonic processing remains the primary dispersion technique for CNTs and other nanoparticles but the rather ad hoc approach to most processes in the literature has major ramifications for reproducibility and dispersion quality. Measurement and control of acoustic cavitation, rather than application of an arbitrary input power, are required to achieve control of nanomaterial dispersion. In the case of CNTs, we conclude that the enhanced exfoliation and length reduction is a result of inertial cavitation, whereas sonochemically induced surface damage is associated with stable cavitation. Dispersion of CNTs in aqueous solution is dominated by mechanical forces generated via inertial cavitation, which depends critically on surfactant concentration. Our approach can be readily generalized to other nanomaterials, for

instance 2D layered materials such as graphene and MoS_2, whose physical and chemical properties are particularly sensitive to number of layers and flake size[1].

From a practical standpoint, careful consideration should be given to container material and vessel geometry when using bath sonication. The use of tip sonication is more challenging due to its intrinsic non-linearity, cavitation shielding effects and volume limitations. For large scale processing, use of a bath vessel with well-controlled and uniform cavitation such as that used in this work is required.

D. CONCLUSIONS

In conclusion, we have developed a new approach for producing a well-characterized acoustic cavitation field during ultrasonication of CNTs, to improve control of dispersion. Through a unique measurement technique, based on *in situ* broadband acoustic emission monitoring and H_2O_2 production, we distinguish between two different cavitation types: (i) stable cavitation, which leads to chemical attack on the CNTs and (ii) inertial cavitation, which favors CNT exfoliation and length reduction. The control of CNT dispersion is more challenging with a tip ultrasonicator due to its intrinsic non-linearity and the presence of cavitation shielding effects. Care must be exercised when using tip-based ultrasonication as the local fields are much higher. We have also highlighted surfactant degradation in the water-surfactant control system in the tens of kHz frequency range used for routine ultrasonication. Furthermore, the surfactant concentration has a profound effect on cavitation activity and resulting dispersion quality via modification of bubble surface tension, radical scavenging and protective coating of CNTs. The

bulk solution temperature increases with time during ultrasonication and has a major influence on the dispersion efficiency through increased vapor pressure and changes in surfactant and bubble dynamics. This study demonstrates that measurement and control of acoustic cavitation rather than blind application of input power is critical in the ultrasonic dispersion of nanomaterials with tailored properties. The results have major implications for enhanced control and scale-up of nanoparticle dispersion using ultrasonic processing.

ACKNOWLEDGMENTS

This work was supported by the U.K. National Measurement System (NMS) under the Innovation R&D Programme and by the U.K. Engineering and Physical Sciences Research Council (EPSRC) under the Industrial Doctorate Engineering Programme in Micro- and NanoMaterials and Technologies at the University of Surrey. The authors thank the following NPL scientific staff members; Dr B. Zeqiri, Dr J. Nunn, Mr C. Allen, Ms T. L. Salter, Dr E. Cerasoli, Dr T. Sainsbury and Dr M. O'Connell for useful discussions and technical assistance in sample preparation and data analysis. Dr J. A. Fagan from the US National Institute of Standards and Technology for contributing the CNTs. Mr D. Lamprou from the University of Surrey for his C.A.D. technical drawing assistance and the NPL reprographics team for their assistance with figures.

SUPPORTING INFORMATION AVAILABLE

Schematic of experimental set up; Additional cavitation measurements; Estimation of effective power; Additional H_2O_2 measurements; Sonochemical degradation of surfactants; Additional

UV-Vis absorption spectroscopy measurements; AFM data analysis. This information is available free of charge via the Internet at http://pubs.acs.org

AUTHOR INFORMATION

Corresponding Author

* E-mail: gareth.hinds@npl.co.uk, Tel. + 44 20 8943 7147

Notes

The authors declare no competing financial interest.

REFERENCES

(1) Coleman, J. N. *et al*. Two-Dimensional Nanosheets Produced by Liquid Exfoliation of Layered Materials. *Science* **2011**, *331*, 568-571.

(2) Nie, Z.; Petukhova, A.; Kumacheva. E. Properties and Emerging Applications of Self-Assembled Structures Made From Inorganic Nanoparticles. *Nature Nanotech*. **2010**, *5*, 15-25.

(3) Tománek, D.; Jorio, A.; Dresselhaus, M. S.; Dresselhaus G. Introduction to Important and Exciting Aspects of Carbon-Nanotube Science and Technology. In *Carbon nanotubes: Advanced Topics In The Synthesis, Structure, Properties And Applications,* Jorio, A., Dresselhaus, M. S., Dresselhaus G., Eds; Topics in Applied Physics 111; Springer-Verlag: Berlin, 2008; pp 1-12.

(4) De Volder, M. F. L.; Tawfick, S. H.; Baughman, R. H.; Hart, A. J. Carbon Nanotubes: Present and Future Commercial Applications. *Science* **2013**, *339*, 535-539.

(5) Schneeweiss, P.; Gierling, M.; Visanescu, G.; Kern, D. P.; Judd, T. E.; Günther, A.; Fortágh, J. Dispersion Forces Between Ultracold Atoms and A Carbon Nanotube. *Nature Nanotech*. **2012**, *7*, 515-519.

(6) Coleman, J. N. Liquid-Phase Exfoliation of Nanotubes and Graphene. *Adv. Funct. Mater.* **2009**, *19*, 3680-3695.

(7) Blanch, A. J.; Lenehan, C. E.; Quinton, J. S. Optimizing Surfactant Concentrations for Dispersion of Single-Walled Carbon Nanotubes in Aqueous Solution. *J. Phys. Chem. B* **2010**, *114*, 9805-9811.

(8) Leighton, T. G. What is Ultrsound?. *Prog. Biophys. Mol. Biol.* **2007**, *93*, 3-83.

(9) Roy, R. A. Cavitation Sonophysics. In *Sonochemistry and Sonoluminescence,* Crum, L. A.; Mason, T. J.; Reisse, J. L.; Suslick, K. S. Eds; Series C: Mathematical and Physical Sciences – vol. 524; Kluwer Academic Publishers: Dordrecht, 1999; pp 25-38.

(10) Lauterborn, W.; Kurz, T. Physics of Bubble Oscillation. *Rep. Prog. Phys*. **2010**, *73*, 106501-106589.

(11) Sutkar, V. S.; Gogate, P. R. Design Aspects of Sonochemical Reactors: Techniques for Understanding Cavitational Activity Distribution and Effect of Operating Parameters. *Chem. Eng.* **2009**, *155*, 26-36.

(12) Pagania, G.; Green, M. J.; Poulin, P.; Pasquali, M. Competing Mechanisms and Scaling Laws for Carbon Nanotube Scission by Ultrasonication. *P. Natl. Acad. Sci USA* **2012**, *109*, 11591-11604.

(13) Green, M. J. Analysis and Measurement of Carbon Nanotube Dispersions: Nanodispersion vs. Macrodispersion. *Polymer. Int.* **2010**, *5*, 1319-1322.

(14) Xu, H.; Zeiger, B. W.; Suslick. K. S. Sonochemical Synthesis of Nanomaterials. *Chem. Soc. Rev*. **2013**, *42*, 2555-2567.

(15) Taurozzi, J. S.; Hackley, V. A.; Wiesner, M. R. Ultrasonic Dispersion of Nanoparticles for Environmental, Health and Safety Assessment-Issues and Recommendations. *Nanotoxicology* **2010**, *5*, 711-729.

(16) Memoli, G.; Gélat, P. N.; Hodnett, M.; Zeqiri, B. Characterisation and Improvement of A Reference Cylindrical Sonoreactor. *Ultrason. Sonochem.* **2012**, *19*, 939-952.

(17) Hodnett, M.; Chow, R.; Zeqiri, B. High-Frequency Acoustic Emissions Generated by A 20 KHz Sonochemical Horn Processor Detected Using A Novel Broadband Acoustic Sensor: A Preliminary Study. *Ultrason. Sonochem.* **2004**, *11*, 441-454.

(18) Ashokkumar, M.; Lee, J.; Kentish, S.; Grieser, F. Bubbles In an Acoustic Field: An Overview. *Ultrason. Sonochem.* **2007**, *14*, 470-475.

(19) Wenseleers, W.; Vlasov, I. I.; Goovaerts, E.; Obraztsova, E. D.; Lobach, A. S.; Bouwen, A. Efficient Isolation and Solubilisation of Pristine Single-Walled Nanotubes in Bile Salt Micelles. *Adv. Funct. Mater.,* **2004**, *14***,** 1105-1112.

(20) SRM®2483 Single-Wall Carbon Nanotubes (Raw soot) Certificate of analysis. Available at:http://www.nist.gov/mml/msed/complex_fluids/nanotube-reference-materials.cfm (August, 2013).

(21) Ashokkumar, M.; Hodnett, M.; Zeqiri, B.; Grieser, F.; Price, G. J. Acoustic Emission Spectra From 515 KHz Cavitation in Aqueous Solutions Containing Surface-Active Solutes. *J. Am. Chem. Soc.* **2007,** *129***,** 2250-2258.

(22) Ashokkumar, M.; Lee, J.; Iida, Y.; Yasui, K.; Kozuka, T.; Tuziuti, T.; Towata A. The Detection and Control of Stable and Transient Acoustic Cavitation Bubbles. *Phys. Chem. Chem. Phys.* **2009**, *11*, 10118-10121.

(23) Blanch, A. J.; Lenehan, C. E.; Quinton, J.S. Parametric Analysis of Sonication and Centrifugation Variables for Dispersion of Single Walled Carbon Nanotubes in Aqueous Solutions of Sodium Dodecylbenzene Sulfonate. *Carbon* 2011, 49, 5213-5228.

(24) Tronson, R.; Ashokkumar, M.; Grieser, F. Comparison of the Effects of Water-Soluble Solutes on Multibubble Sonoluminescence Generated In Aqueous Solutions by 20- and 515-KHz Pulsed Ultrasound. *J. Phys. Chem. B* **2002**, *106*, 11064-11068.

(25) Sostaric, J. Z.; Riesz, P. Adsorption of Surfactants at the Gas-Solution Interface of Cavitation Bubbles: An Ultrasound Intensity-Independent Frequency Effect in Sonochemistry. *J. Phys. Chem. B* **2002**, *106*, 12537-12548.

(26) Destaillats, H.; Hung, H. M.; Hoffmann, M. R. Degradation of Alkyphenol Ethoxylate Surfactants in Water with Ultrasonic Irradiation. *Environ. Sci. Tech.* **2000**, *34*, 311-317.

(27) Angelikopoulos, P.; Bock H. The Science of Dispersing Carbon Nanotubes with Surfactants. *Phys. Chem. Chem. Phys.* **2012**, *14*, 9546-9557.

(28) Mukherjee, P.; Padhan, S. K.; Dash, S.; Patel, S.; Mishra, B. K. Clouding Behaviour in Surfactant Systems. *Adv. Colloid Interface Sci.* **2011**, *162*, 59-79.

(29) Naumov,A.; Ghosh, V. S.; Tsyboulski, D. A.; Bachilo, S. M.; Weisman, R. B. Analyzing Absorption Backgrounds in Single-Walled Carbon Nanotube Spectra. *ACS Nano* **2011**, *5*, 1639-1648.

(30) Tan,Y.; Resasco, D. E. Dispersion of Single-Walled Carbon Nanotubes of Narrow Diameter Distribution. *J. Phys. Chem. B* **2005**, *109*, 14451-14460.

(31) Jorio, A.; Dresselhaus, M. S.; Saito, R.; Dresselhaus, G. *Raman Spectroscopy in Graphene Related Systems,* Wiley-VCH, Weinheim, Germany, 2011.

(32) Fenoglio, I.; Tomatis, M.; Lison, D.; Muller, J.; Fonseca, A.; Nagy, J. B.; Fubini, B. Reactivity of Carbon Nanotubes: Free Radical Generation or Scavenging Activity? *Free Radical Biol. Med.* **2006**, *40*, 1227-1233.

(33) Cançado, L. G. *et al*. Quantifying Defects in Graphene via Raman Spectroscopy at Different Excitation Energies. *Nano Lett.* **2011**, *11*, 3190-3196.

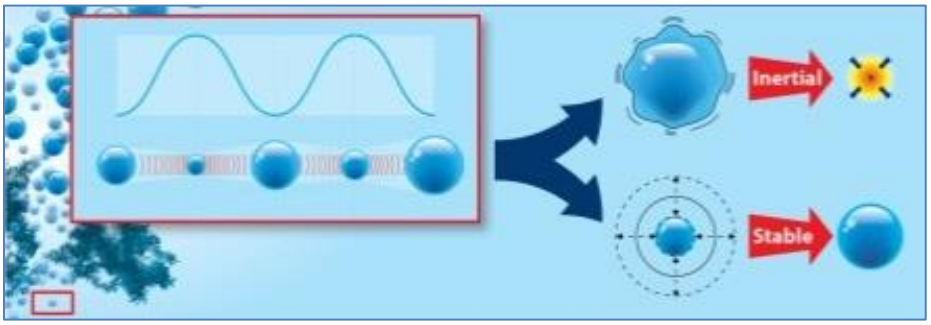
Inertial
Stable

Supporting Information

Influence of Acoustic Cavitation on the Controlled Ultrasonic Dispersion of Carbon Nanotubes

Achilleas Sesis[†], *Mark Hodnett*[†], *Gianluca Memoli*[†], *Andrew J. Wain*[†], *Izabela Jurewicz*[‡], *Alan B. Dalton*[‡], *J. David Carey*[§] *and Gareth Hinds*[†*]

[†]National Physical Laboratory, Teddington, Middlesex, TW11 0LW, United Kingdom

[‡]Department of Physics, University of Surrey, Guildford, Surrey, GU2 7XH, United Kingdom

[§]Advanced Technology Institute, University of Surrey, Guildford, Surrey, GU2 7XH, United Kingdom

1. Schematic of experimental set up

The experimental set up of the reactor during ultrasonic treatment is shown schematically in Figure S1. Figure S1a illustrates the reactor/reference vessel configuration and Figure S1b the reactor/sonotrode configuration. During experiments only the top row of transducers was used with the applied nominal power evenly distributed between all ten transducers.

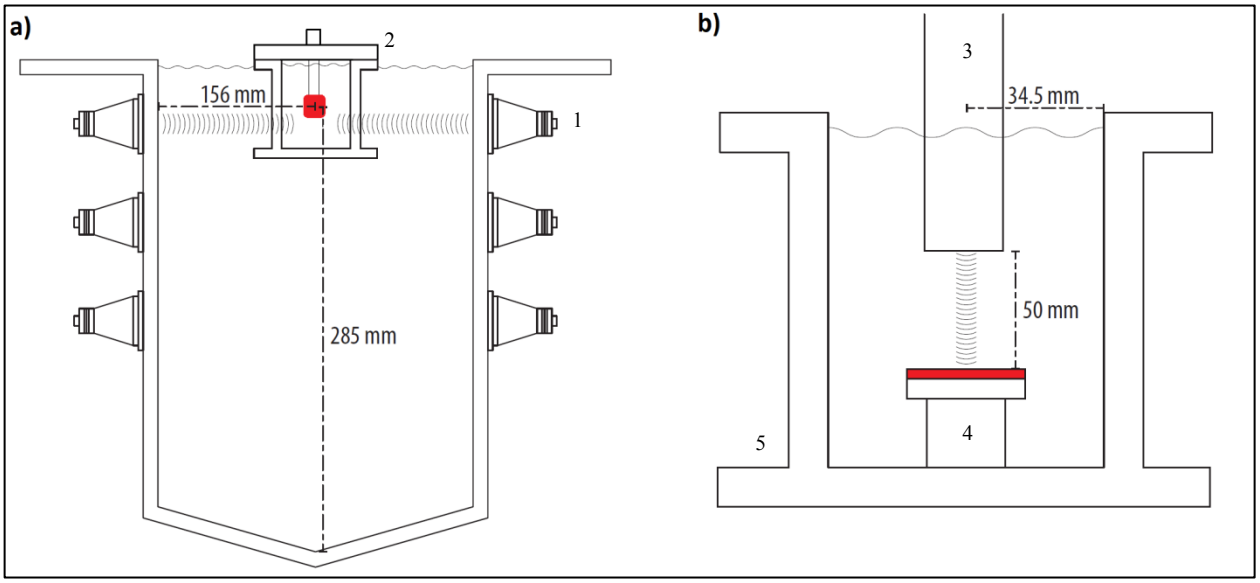

Figure S1 Reactor/reference vessel (a) and reactor/sonotrode (b) configuration. Red shading indicates the position of the sensor. (1) transducers; (2) enclosed reactor; (3) sonotrode; (4) sensor holder and (5) open top reactor. Image not to scale.

2. Additional cavitation measurements

Figures S2(a)-(f) show the variation of E_{cav} with time under the conditions required to complete the matrix of experimental variables studied in this work, i.e. input power, surfactant concentration and the presence or absence of CNTs.

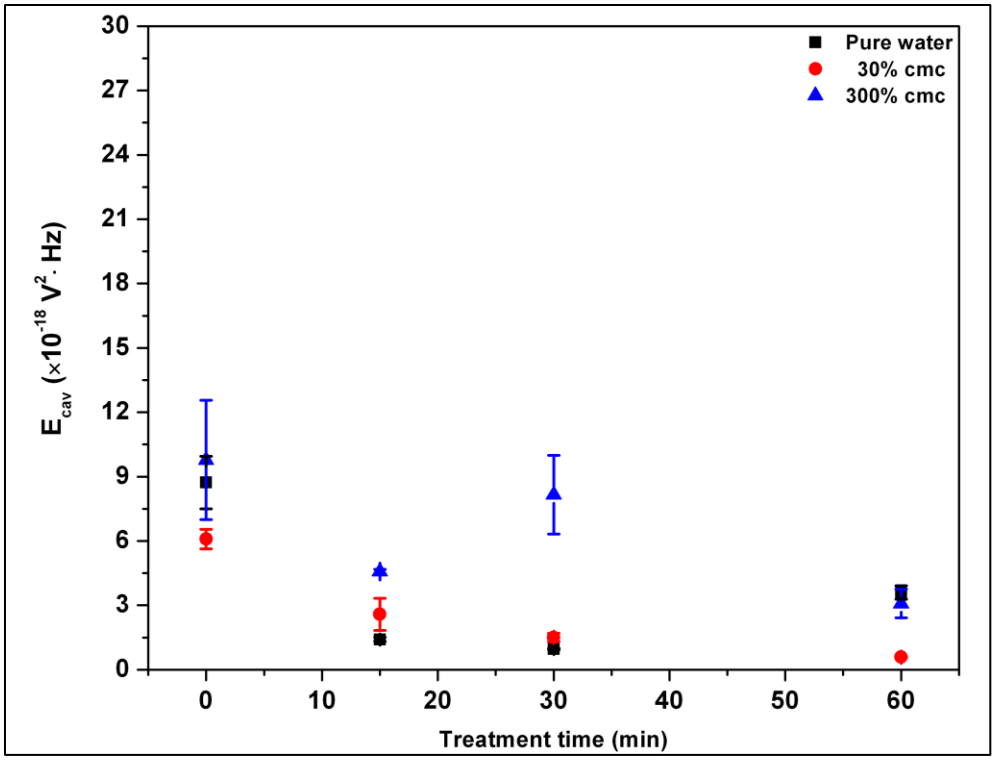

Figure S2a Summary of the acoustic measurements for the solutions treated at 100 W. Error bars represent standard error between four to eight independent measurements.

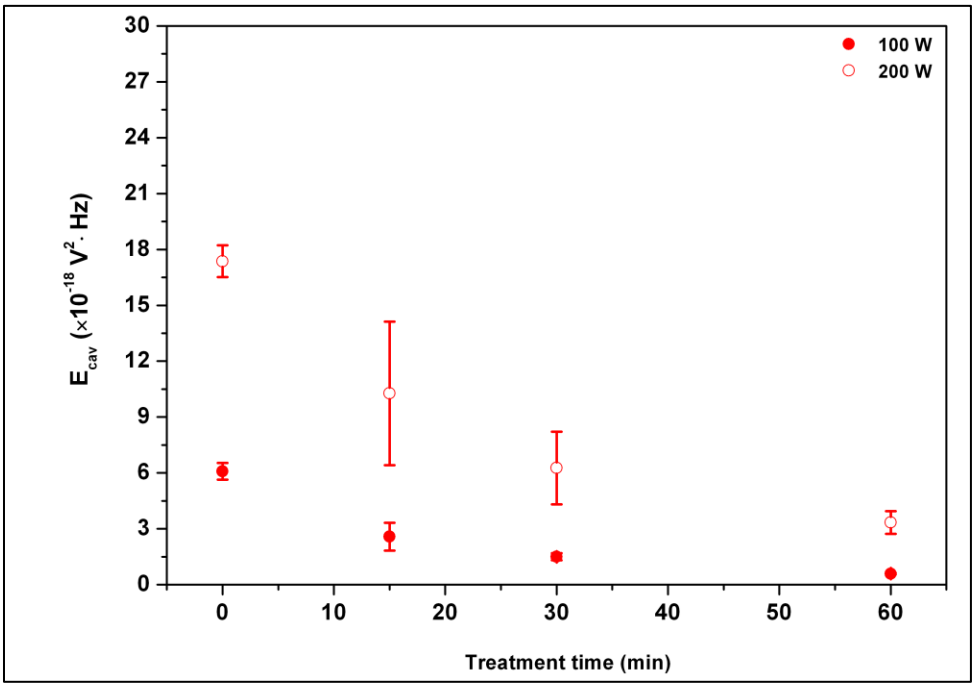

Figure S2b Effect of input power on acoustic measurements for the 30% cmc solution. Error bars represent standard error between four to eight independent measurements.

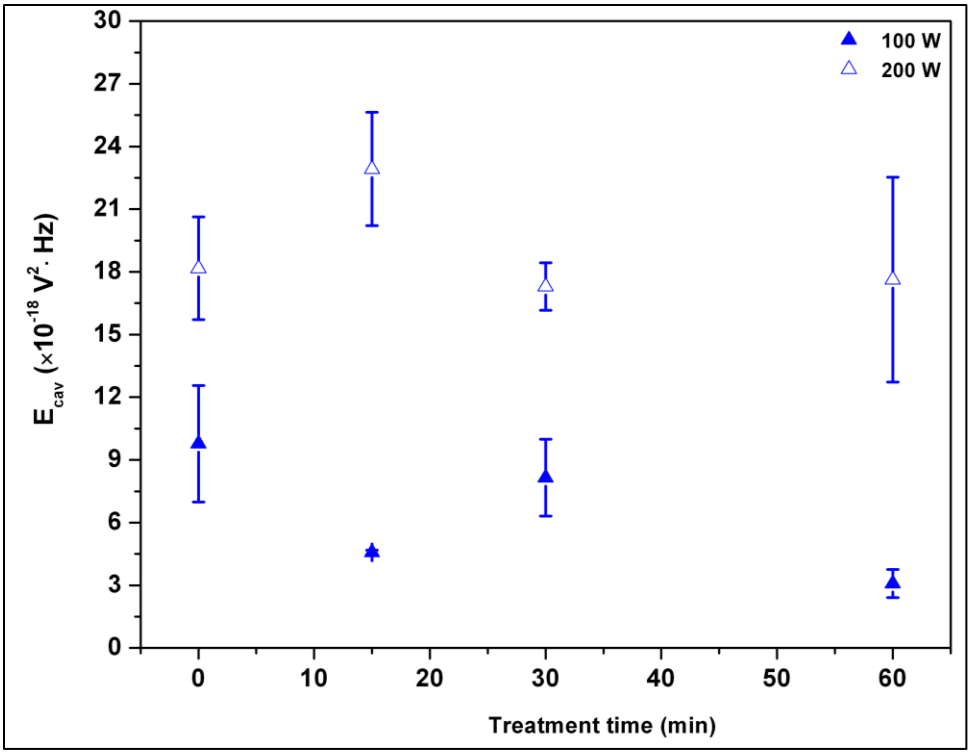

Figure S2c Effect of input power on acoustic measurements for the 300% cmc solution. Error bars represent standard error between four to eight independent measurements.

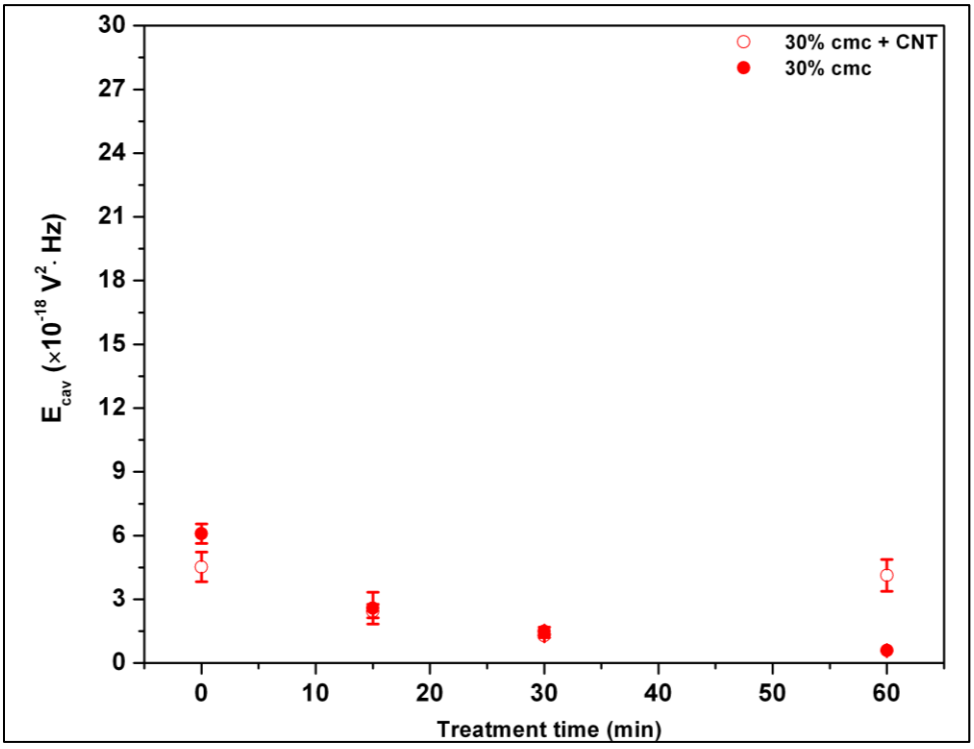

Figure S2d Acoustic measurements for the 30% cmc solutions without and with CNTs (0.02 mg mL^{-1}) treated at 100 W. Error bars represent standard error between four to eight independent measurements.

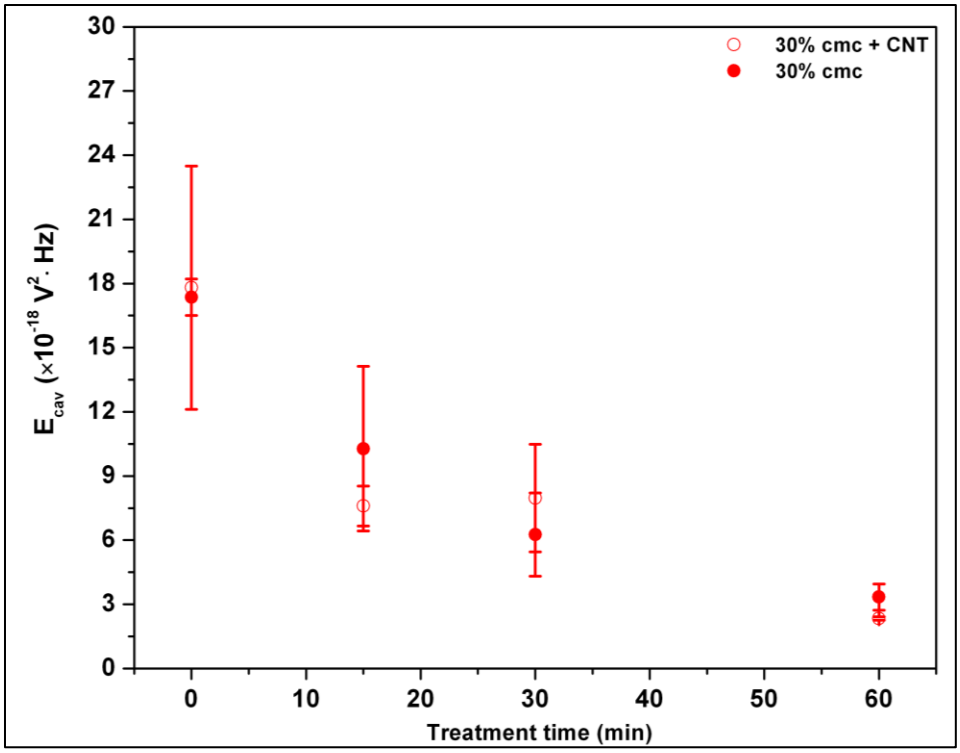

Figure S2e Acoustic measurements for the 30% cmc solutions without and with CNTs (0.02 mg mL^{-1}) treated at 200 W. Error bars represent standard error between four to eight independent measurements.

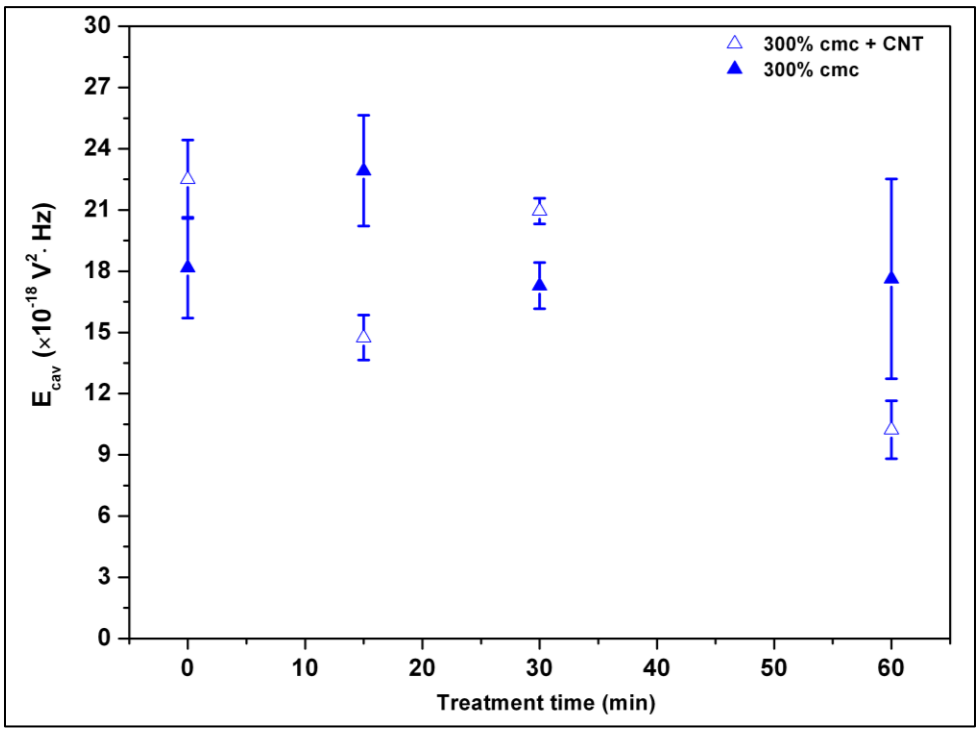

Figure S2f Acoustic measurements for the 300% cmc solutions without and with CNTs (0.02 mg mL^{-1}) treated at 200 W. Error bars represent standard error between eight independent measurements.

3. Estimation of effective power

The effective power applied to the sonoreactor during the acoustic experiments can be estimated by calorimetry. Average thermographs from all of the tests are shown at both 100 W (Figure S3) and 200 W (Figure 3). Rates of temperature increase ($\frac{dT}{dt}$) of 0.02°C s^{-1} (100 W) and 0.03°C s^{-1} (200 W) are observed before reaching a plateau indicative of thermal equilibrium. Using Equation S1 an approximate value of the delivered acoustic power (effective power, P_{ef} in W) can be calculated.

$$P_{ef} = \frac{dT}{dt}\, mC_p \tag{S1}$$

where $C_p = 4180\, J\, kg^{-1}\, K^{-1}$ is the specific heat capacity of water at 20 °C and $m = 0.250\, kg$ is the mass of liquid in the sonoreactor. This yields an effective power of 21 W (for an input power of 100 W) and 31 W (for an input power of 200 W), demonstrating the nonlinear dependence of effective power on input power. The insets in Figure S3 and Figure 3 show the average trend line of temperature of the water in the 25 L vessel with time, with rates of temperature increase of 1.3×10^{-4} °C s^{-1} (100 W) and 1.8×10^{-4} °C s^{-1} (200 W). Application of Equation S1 shows that the effective power dissipated in the reference vessel is 14 W (at 100 W) and 19 W (at 200 W). This gives a total dissipated power in the water phase of 35 W (at 100 W) and 50 W (at 200 W), indicating that the majority of the loss in power is through air-cooling of the transducers.

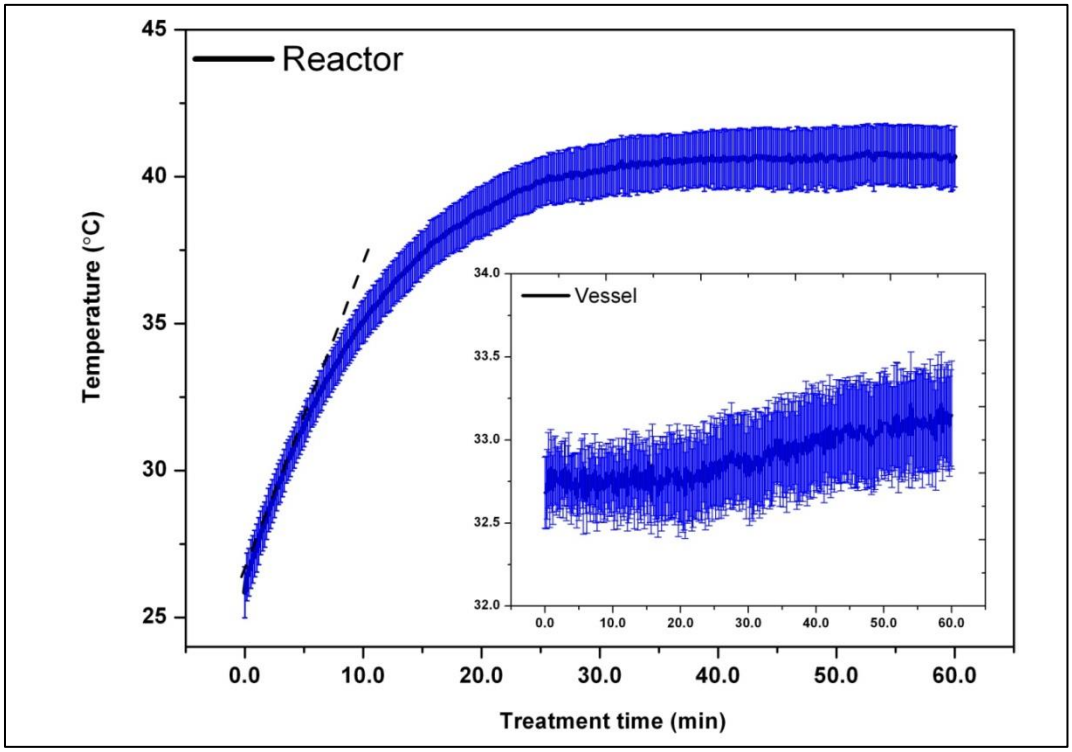

Figure S3 Average thermographs of the temperature within the reactor during the 100 W tests. Inset illustrates the vessel temperature profile. Error bars represent standard error between six independent measurements.

4. Additional H_2O_2 measurements

Figures S4(a)-(e) show the variation of hydrogen peroxide concentration with time under the conditions required to complete the matrix of experimental variables studied in this work, i.e. input power, surfactant concentration and the presence or absence of CNTs.

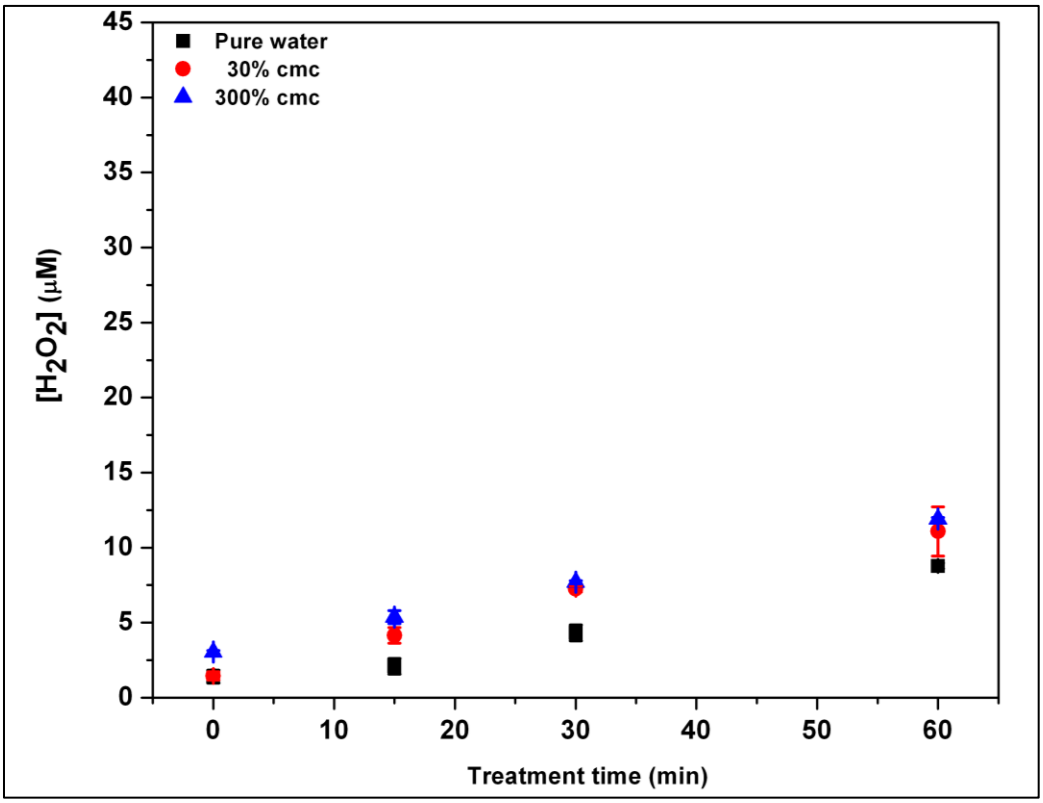

Figure S4a Measurements of H_2O_2 concentration at 100 W for the 30% cmc and 300% cmc solutions. Error bars represent standard error between four independent measurements.

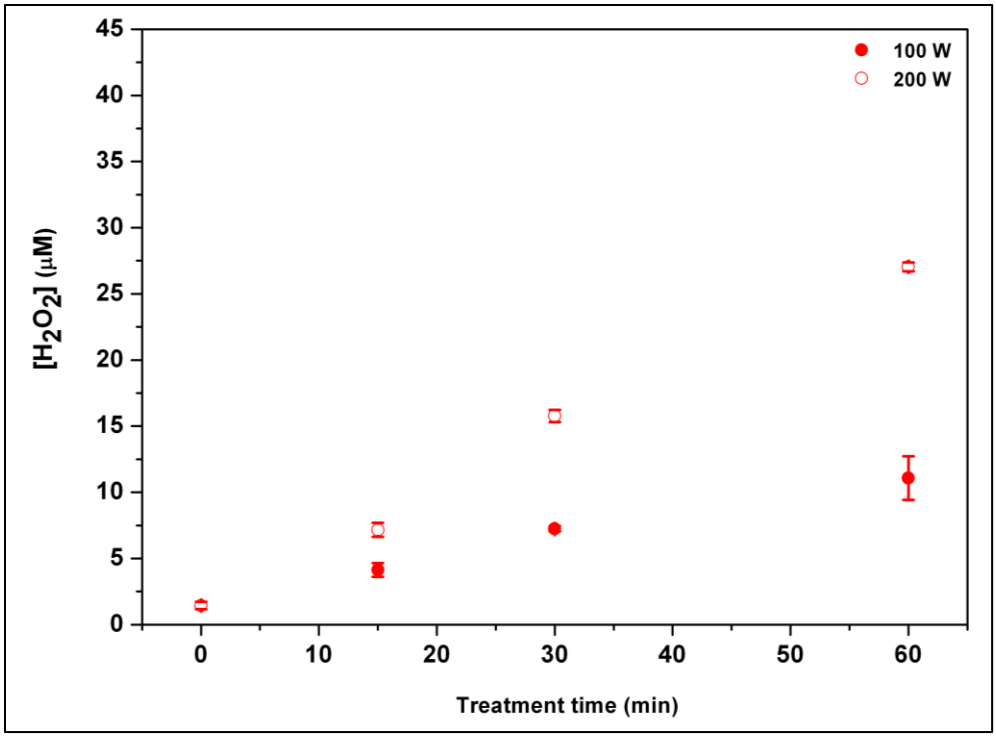

Figure S4b Measurements of H_2O_2 concentration at 100 W and 200 W for the 30% cmc solutions. Error bars represent standard error between four independent measurements.

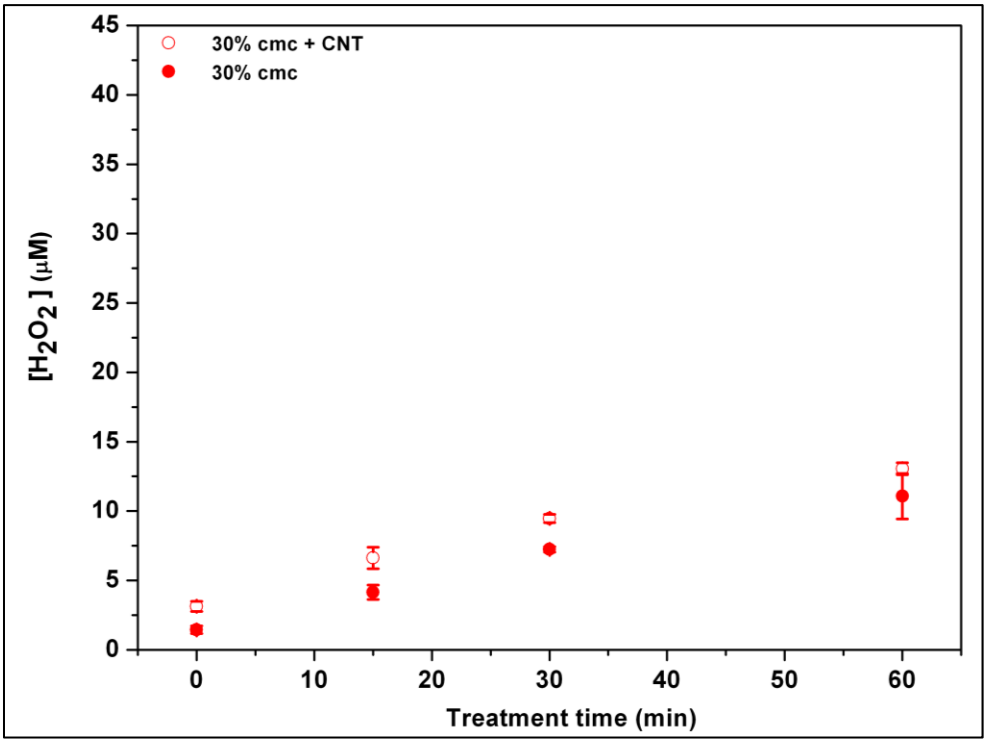

Figure S4c Measurements of H_2O_2 concentration at 100 W for the 30% cmc solutions without and with CNTs (0.02 mg mL^{-1}). Error bars represent standard error between four independent measurements.

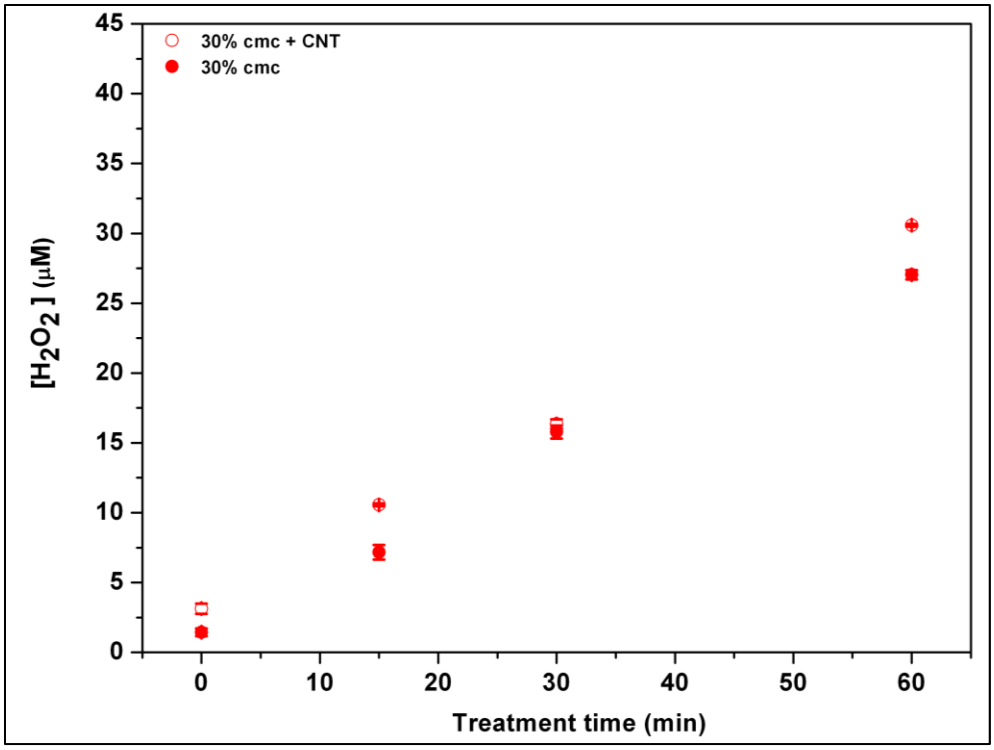

Figure S4d Measurements of H_2O_2 concentration at 200 W for the 30% cmc solutions without and with CNTs (0.02 mg mL^{-1}). Error bars represent standard error between four independent measurements.

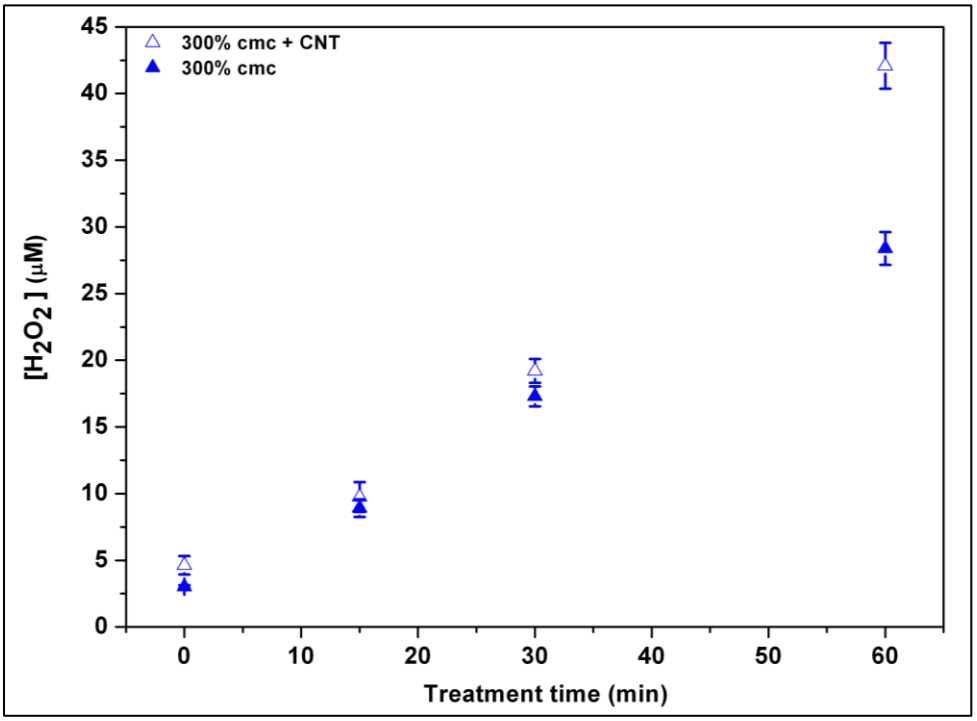

Figure S4e Measurements of H_2O_2 concentration at 200 W for the 300% cmc solutions without and with CNTs (0.02 mg mL^{-1}). Error bars represent standard error between four independent measurements.

5. Sonochemical degradation of surfactants.

Table S1 shows the degradation products of surfactant as a function of input power and exposure time. Estimates of molecular fragment structure were performed using XCalibur™ (Thermo Scientific) software set to a mass accuracy of 5 ppm. Examples of the HPLC trace for TX are depicted for various ultrasonic treatments in Figure S5. Multiple peaks are observed signifying the various lengths of the polyoxyethylene group (*n*). The reduction in absorbance as a function of treatment time is due to the ultrasonically induced degradation of the TX molecule.

Table S1 Relative intensities of ion species (× 1000) detected using ESI-MS. Shaded box indicates the molecular ion of the parent NaDOC molecule.

$[m+H]^+$	0 W - 0 min	100 W - 30 min	200 W - 30 min	200 W - 60 min	Chemical Composition
283.225		246	538	1001	$C_{15}H_{31}O_3Na$
355.264		313	487	711	$C_{24}H_{34}O_2$
373.274	233	527	857	1162	$C_{24}H_{36}O_3$
389.269		496	962	1220	$C_{24}H_{36}O_4$
391.285		434	831	1059	$C_{24}H_{38}O_4$
413.267		491	588	986	$C_{24}H_{37}O_4Na$
415.282	2821	3637	2371	2152	$C_{24}H_{39}O_4Na$

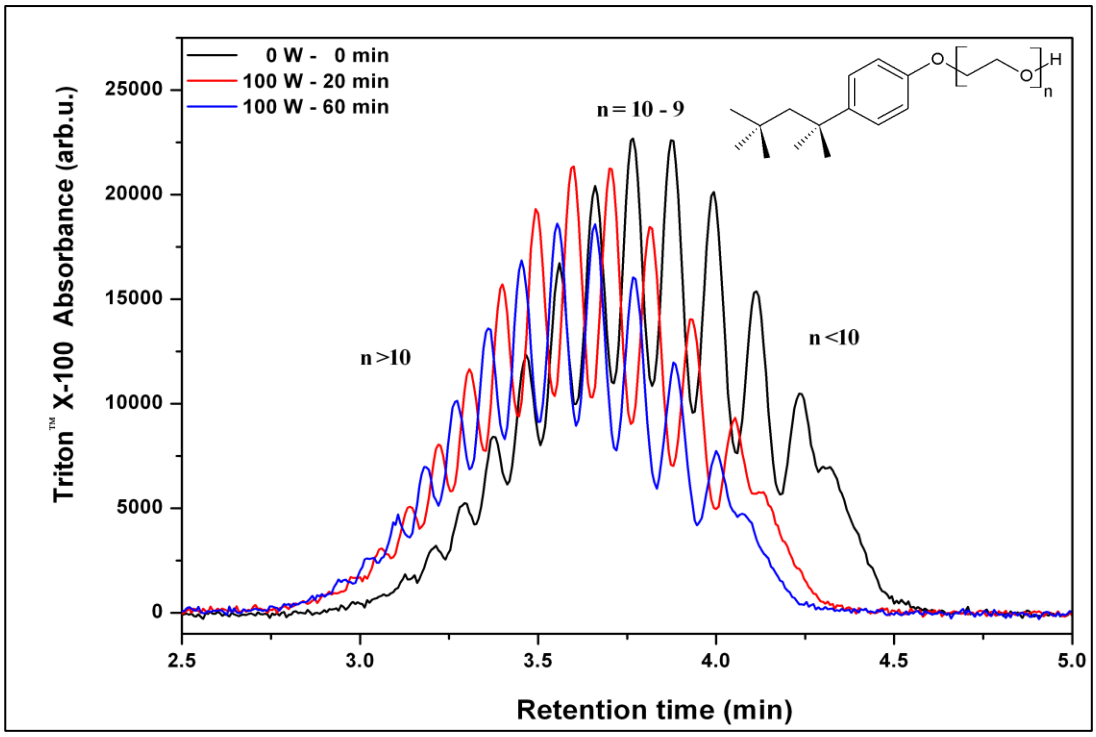

Figure S5 HPLC-RP chromatograph for Triton™ X-100. Inset illustrates the TX molecular structure.

6. Additional UV-Vis absorption spectroscopy measurements

In Figure S6a the ratio of the E_{22} (570 nm) peak to its respective non-resonance background is presented for CNT solutions (surfactant concentration 30% cmc and 300% cmc) treated at 100 W. The ratios are calculated based on the description by Tan *et al*[30]. In Figure S6b and S6c linear fits between 15 and 60 minutes are used to calculate the gradient, which serves as a relative efficiency indicator.

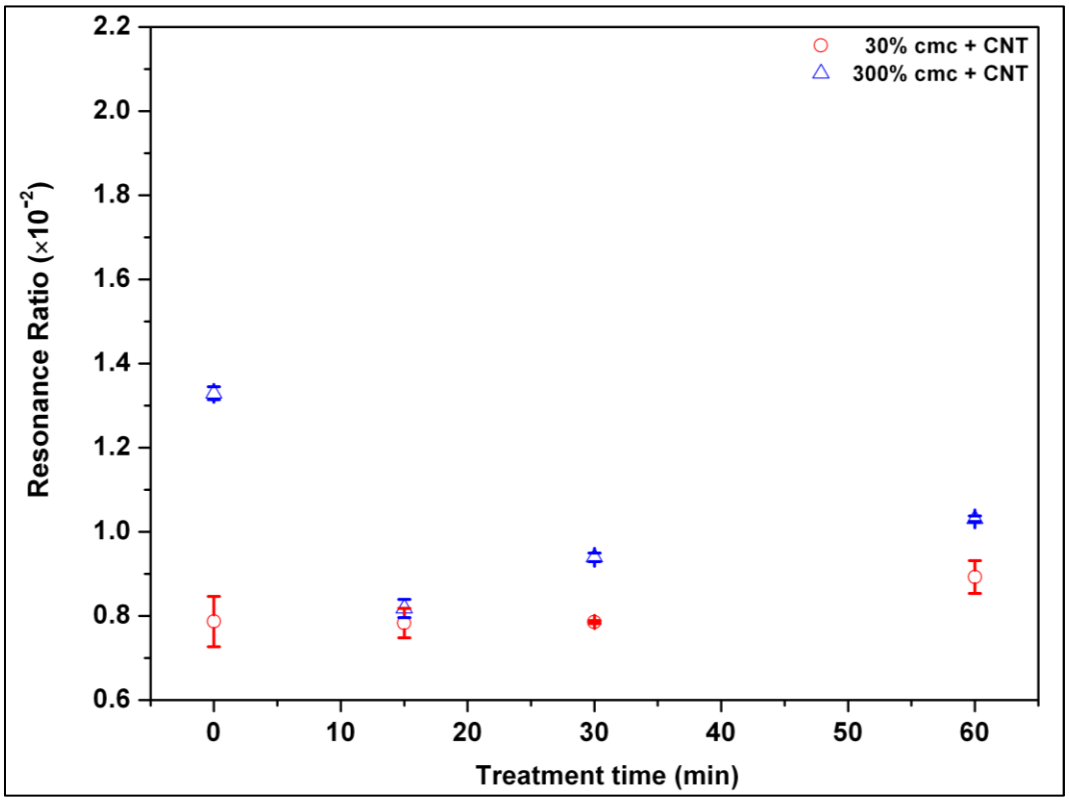

Figure S6a E_{22} resonance ratios of CNTs treated at 100 W in 30% and 300% cmc solutions. Error bars represent standard error between four independent measurements.

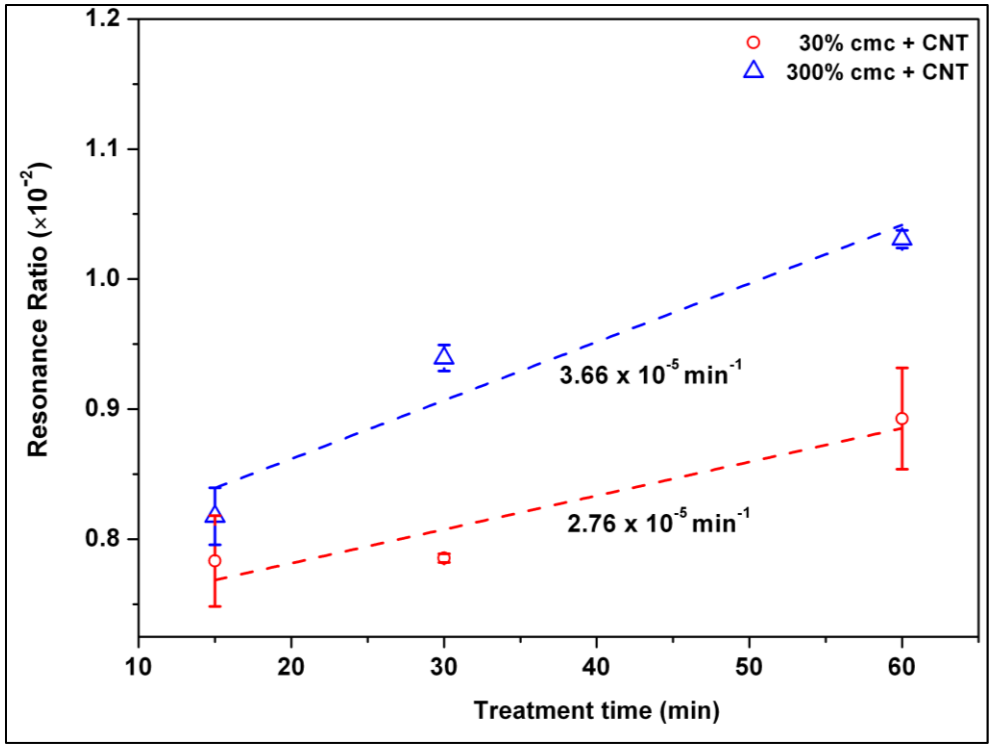

Figure S6b E_{22} resonance ratios of CNTs treated at 100 W in 30% and 300% cmc solutions. Error bars represent standard error between four independent measurements.

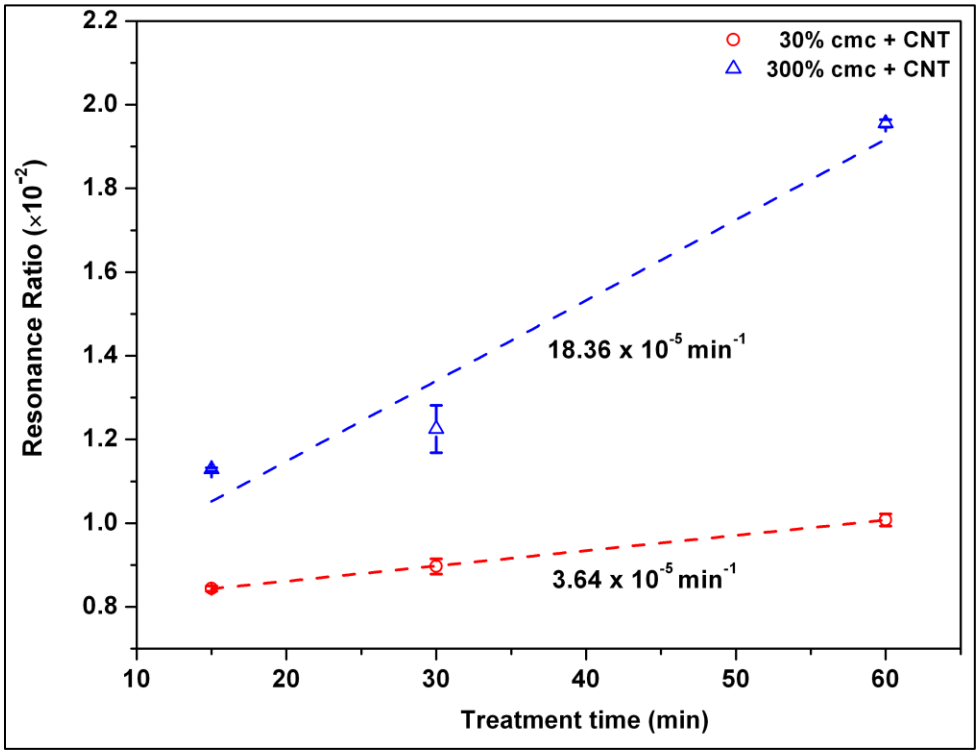

Figure S6c E_{22} resonance ratios of CNTs treated at 200 W in 30% and 300% cmc solutions. Error bars represent standard error between four independent measurements.

7. AFM data analysis

Averaged data from AFM measurements are plotted in Figure S7a and S7b. As indicated by the blue dashed arrow, increasing both ultrasonic treatment time and power results in a greater degree of CNT exfoliation and length reduction in the 300% cmc solution compared to the 30% cmc solution. Only lengths of CNTs below 1.00 nm in diameter were included.

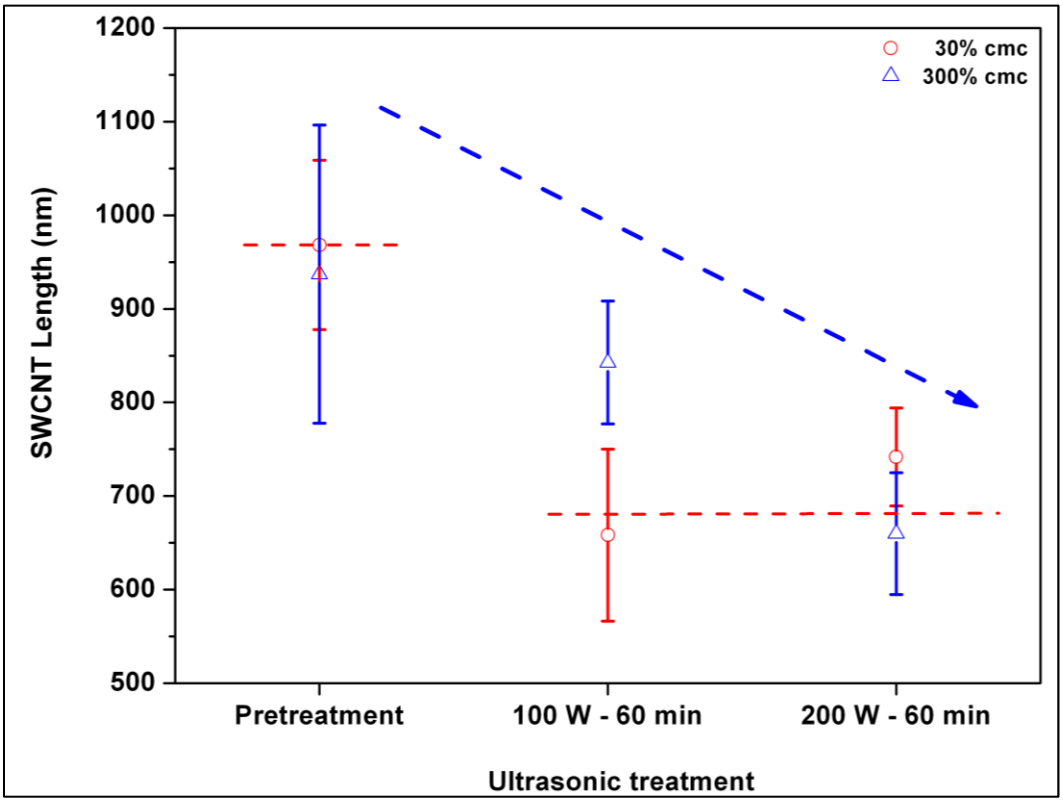

Figure S7a Effect of ultrasonic treatment on CNT length. Error bars represent standard error between 150 independent measurements.

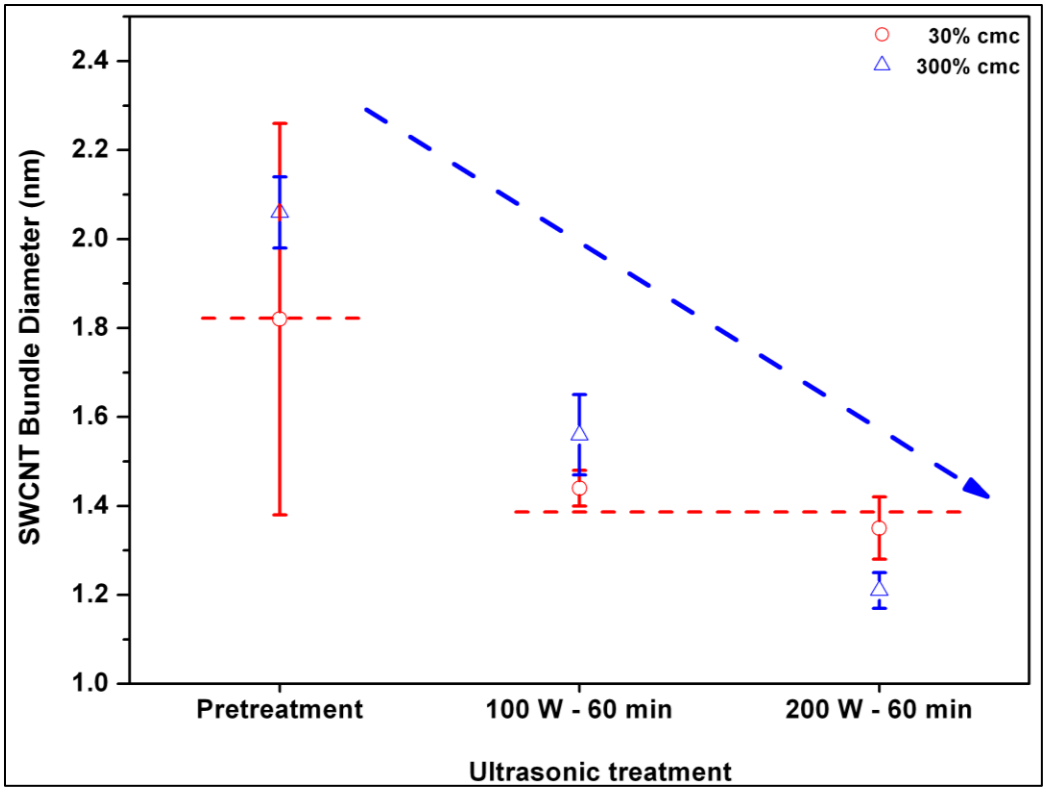

Figure S7b Effect of ultrasonic treatment on CNT diameter. Error bars represent standard error between 150 independent measurements.